Ecological Informatics 31 (2016) 59–69

Contents lists available at ScienceDirect

Ecological Informatics

journal homepage: www.elsevier.com/locate/ecolinf

Modeling the interplay between deepwater oxygen dynamics and sediment diagenesis in a hard-water mesotrophic lake

Alex Gudimov, Jalene McCulloch, Jianwen Chen, Phuong Doan, George Arhonditsis, Maria Dittrich *

Department of Physical and Environmental Sciences, University of Toronto Scarborough, 1265 Military Trail, Toronto, ON M1C 1A4, Canada

ARTICLE INFO

Article history:
Received 23 July 2015
Received in revised form 12 November 2015
Accepted 15 November 2015
Available online 21 November 2015

Keywords:
Sediment diagenesis
Reactive-transport model
Hypoxia
Sediment oxygen demand
Lake Simcoe

ABSTRACT

Sediment diagenesis can be a significant driver of oxygen depletion in lakes and may dramatically impact the hypolimnetic oxygen concentrations. In this study, our aim is to simulate sediment oxygen demand (SOD) dynamics under varying conditions of organic matter sedimentation and hypolimnetic oxygen levels. Specifically, we use a process-based sediment diagenesis model to identify the critical processes that regulate dissolved oxygen levels in the hypolimnion of the mesotrophic Lake Simcoe, Ontario, Canada. We quantify the spatial distribution of organic matter mineralization and subsequently assess the role of sediment oxygen demand in hypolimnetic oxygen depletion. Our model reinforces the notion that aerobic mineralization is a major diagenetic process that shapes sediment oxygen demand in the system. Our model confirms existing empirical evidence that SOD contribution to the hypolimnetic oxygen deficit is less than 30% in Lake Simcoe. Our analysis also sheds light on the potential drivers of the significant spatial heterogeneity of the sediment oxygen demand among Kempenfelt Bay, Cook's Bay, and the main basin of Lake Simcoe, namely, the differences in primary production rates, the origins of the settling organic matter, the redistribution of sediments, and the oxygen concentration at the sediment–water interface due to differences in morphology and hydrodynamics. We conclude by arguing that the pace of the planned re-oligotrophication and the anticipated hypolimnetic oxygen improvements, induced by nutrient loading reductions, may experience short-term delays from years to several decades due to the potential effects of a number of feedback mechanisms across the sediment–water interface in Lake Simcoe.

1. Introduction

The tight linkage between lake productivity and hypolimnetic dissolved oxygen (DO) concentration is well established in deep stratified lakes (Wetzel, 2001). Elevated lake productivity and organic matter (OM) sedimentation lead to anoxic conditions in deepwaters, which subsequently induce excessive release of nutrients from the sediments as well as accumulation of metals/toxic substances (e.g., methane, ammonium, and sulfide) near the lake bottom (Carignan and Lean, 1991; Gelda et al., 1995). Sediment oxygen demand (SOD) in lakes can be connected to both autochthonous and allochthonous OM loading rates and may significantly impact the rate of hypolimnetic DO depletion along with the oxygen penetration depth (OPD) in the sediments (Katsev et al., 2007; Matzinger et al., 2010; Müller et al., 2012). Besides the toxic impact of substances released from sediments on benthic organisms, the occurrence and extension of anoxic deepwater zones poses constraints on the integrity of fish habitats, especially those for cold-water species (Wu et al., 2003; Evans, 2007).

Because of the dire ramifications of hypoxia, lake management often revolves around the establishment of hypolimnetic DO threshold concentrations in deepwaters, e.g., <2–4 mg L^{-1}. Various strategies have been developed to meet such targeted hypolimnetic DO levels, including the reduction of external nutrient loading (Gächter and Wehrli, 1998), deepwater oxygenation (Liboriussen et al., 2009), aeration or mixing in winter (Mueller and Stadelmann, 2004), and removal of sediments containing high amount of organic matter (Annadotter et al., 1999). However, the effects of these restoration strategies are often delayed (Mueller and Stadelmann, 2004; Liboriussen et al., 2009). In other instances, decline in primary production/organic carbon sedimentation and ultimately hypoxia alleviation are only observed after a disproportional reduction of external nutrient loading (Charlton et al., 1993; Matthews and Effler, 2006). Importantly, SOD can drive hypolimnetic DO deficit for decades after lake re-oligotrophication, also known as the "sediment memory effect" (Gelda et al., 2012a, 2012b). The reason for the latter pattern is the slow degradation of accumulated OM from past periods of eutrophication coupled with the diffusion of degradation products from the sediments to the water column. For example, Carignan and Lean (1991) found that the degradation of the refractory portion of deposited OM to reduced substances could last from decades to centuries. Thus, detailed knowledge of the processes occurring within the top few centimeters of the sediment is essential for assessing water quality conditions, understanding the manifestation of hypoxia, and the management of surface waters.

* Corresponding author. Tel.: +1 416 208 2786; fax: +1 416 287 7279.
E-mail address: mdittrich@utsc.utoronto.ca (M. Dittrich).

http://dx.doi.org/10.1016/j.ecoinf.2015.11.005
1574-9541/

Diagenetic modeling is an indispensable tool to investigate the interplay among the sediment diagenesis processes, to generate hypotheses about the sediment–water column coupling, and to predict potential ecosystem behaviors. The demand for robust sediment diagenesis predictions is often underscored as a focal point when attempting to elucidate future lake hypoxia patterns and to gain insights into sediment functioning under projected changes in lake trophic status (Zhang and Arhonditsis, 2008). Nonetheless, this type of process-based diagenetic modeling as well as the data that necessitate to ground-truth those models (e.g., depth profiles of concentrations of dissolved and solid substances, phosphorus binding forms, organic matter depth profiles) are still missing in the context of water quality management (Smits and van Beek, 2013; Paraska et al., 2014). For example, existing sediment modeling studies have profoundly overlooked critical mechanisms, such as the diffusive boundary layer conditions (Brand et al., 2009) or the macrophyte subsidies to OM pool, while others lacked essential features in their configuration, such as flexible sediment depth profiles, dynamic behavior of forcing conditions in lake sediments, and lateral variability of sediment parameter vectors (see review by Paraska et al., 2014). In the same context, Kim et al. (2013) emphatically argued that field, experimental, and modeling work should be designed to shed light on the mechanisms of nutrient mobilization in the sediments and to identify process controls under a variety of conditions. The knowledge obtained from process-based diagenetic modeling will allow addressing research questions, such as the following: Can nutrient retention in lake sediments be predicted based on the sediment mineralogy, sedimentation substance inputs, catchment type, and other characteristics? How does sediment retention capacity with respect to nutrients respond to changes caused by human activities and/or climate change?

Recognizing the importance of the dynamic nature of diagenetic processes in lake sediments, the present study is founded upon a 1-D non-steady-state reaction-transport model for Lake Simcoe, Ontario, Canada (McCulloch et al., 2013). Lake Simcoe has experienced varying degrees of eutrophication problems since the establishment of the first European settlers in the 17th century (North, 2013). Increasing urbanization, intensive agricultural practices, atmospheric deposition, and internal and multiple external phosphorus loading have impacted the ecological health of the lake system (Gudimov et al., 2012). The depletion of hypolimnetic DO following eutrophication has been identified as a main reason for the recent collapse in cold-water fishery recruitment (Young et al., 2011). In this study, our intent is to quantify the contribution of the sediments to hypolimnetic DO depletion as well as to investigate the impact of OM loading on seasonal SOD dynamics and sediment diagenesis processes in three basins of Lake Simcoe. We also explicitly accommodate the lateral heterogeneity of the processes associated with the oxygen demand, thereby challenging the validity of model parameterizations that postulate spatial homogeneity. Finally, we conduct local sensitivity analysis to identify critical processes at the sediment–water interface or near-bottom conditions that may shape O_2 concentration profiles in sediments.

2. Methods

2.1. Study site and experimental data

Lake Simcoe is located 44 km north of Toronto with 11.6 km^3 of water volume and a catchment area of 2,840 km^2 (Fig. 1a). It is a dimictic lake that completely freezes over during most winters. In its current mesotrophic state, Lake Simcoe receives wastewater from fourteen municipal wastewater treatment plants, which constitute sources of phosphorus (P) loading (6 ± 1 tonnes $year^{-1}$ between 2004 and 2007) and substantial phosphorus loads are also deposited from the atmosphere (18 ± 4 tonnes $year^{-1}$) or emanate from other non-point sources, including runoff from agricultural, urban and natural areas (43 ± 5 tonnes $year^{-1}$), and rural septic systems (4.4 ± 0.1 tonnes $year^{-1}$) (Table 1; see also Gudimov et al., 2012). Lake Simcoe consists of a large main basin (mean depth 14 m, maximum depth 33 m) and two large bays: the narrow and deep Kempenfelt Bay on the west side of the lake (area 34 km^2, mean depth 20 m) and the shallow Cook's Bay at the south end of the lake (area 44 km^2, mean depth 13 m). Cook's Bay is connected to Holland Marsh, an agricultural cluster of artificially reclaimed land, rich with organic matter, through dikes and drainage canals, while the Kempenfelt Bay subwatershed is the location of the city of Barrie, where a population of about 135,000 inhabitants resides.

The sediment data set for model calibration was collected in spring and autumn of 2011 from three basins of the lake, i.e., sites K42, K45, and C9 (Fig. 1a; see detailed description in Dittrich et al., 2013). In short, sediment samples of 60 cm length were collected using a core sampler. Microsensor measurements for O_2 and pH were carried out immediately upon arrival to the laboratory. Two cores were used for pore water analysis, and two to three cores were used for the fractionation of phosphorus, porosity analysis, dry weight, and total organic matter. The historical DO profiles in the water column (Fig. 1b) were provided by the Ontario Ministry of the Environment (personal communication Dr. Hamdi Jarjanazi). Historical sedimentation fluxes follow the Hiriart-Baer et al. (2011) dating results. The lake hypolimnetic area during the summer-stratified period refers to layers of the water column below 18 m depth (Young et al., 2011). A P sequential extraction analysis quantified the P pools in the sediments, including mobile pool, which suggested a distinct heterogeneous pattern of the P-binding forms in Lake Simcoe (Dittrich et al., 2013). In Cook's Bay, the predominant fraction of total phosphorus (TP) is carbonate-bound P (apatite-*P*) mainly due to the accelerated erosion in the catchment. TP content in the sediments of Cook's Bay is the lowest among the three studied basins in Lake Simcoe, providing evidence that the high sedimentation rates and natural watershed sources may lead to a "dilution" of *P* in the sediment dry matter. In contrast, the hypolimnetic sediments in Kempenfelt Bay are responsible for high diffusive *P* fluxes into the water column, presumably reflecting the highest proportion of the redox-sensitive *P* sediment pool compared to other lake segments as well as the occasional hypoxic conditions in the Kempenfelt Bay hypolimnion (Eimers et al., 2005). The sediments in the main basin are mostly driven by fast diagenetic processes of settling organic matter from lake epilimnion, which may lead to internal *P* loading greater than 9 tonnes *P* $year^{-1}$ (Gudimov et al., 2015). Further details regarding the sampling practices and analytical protocols can be found in Dittrich et al. (2013).

2.2. Model description and implementation

The diagenetic model for Lake Simcoe was developed using AQUASIM software in 1-D reactive-transport sediment compartment for solid and dissolved substances (Reichert, 1998; Dittrich et al., 2009). The model accounted for deposition fluxes of particulate matter, sediment compaction, bioturbation/bioirrigation, solute molecular diffusion, primary and secondary redox reactions, mineral precipitation/dissolution and acid dissociation reactions (McCulloch et al., 2013; see also Table S1). The sediment model is based on mass-conservation diagenetic equations for solid and dissolved substances (Berner, 1980):

$$\frac{\partial(\theta S_i)}{\partial t} = \frac{\partial}{\partial z}\left(D_b \frac{\partial(\theta S_i)}{\partial z} + \theta D_{Si} \frac{\partial S_i}{\partial z}\right) + r_{S_i} - \alpha_{\text{bioirrig}} \theta \left(S_i - S_i^{\text{SWI}}\right)$$

$$\frac{\partial(X_i)}{\partial t} = \frac{\partial(v_{\text{sed}} X_i)}{\partial z} + \frac{\partial}{\partial z}\left(D_b \frac{\partial(X_i)}{\partial z}\right) + r_{x_i}$$

where X_i and S_i represent solid and dissolved phase species, θ is the porosity, z is the vertical dimension of the sediment core, t is time, r_{Si} and r_{Xi} are the biogeochemical transformation rates and v_{sed} is the velocity of sediment vertical movement, D_{Si} is the solute molecular diffusion, D_b is the bioturbation coefficient, a_{bioirrig} is the bioirrigation coefficient, S_i^{SWI} is

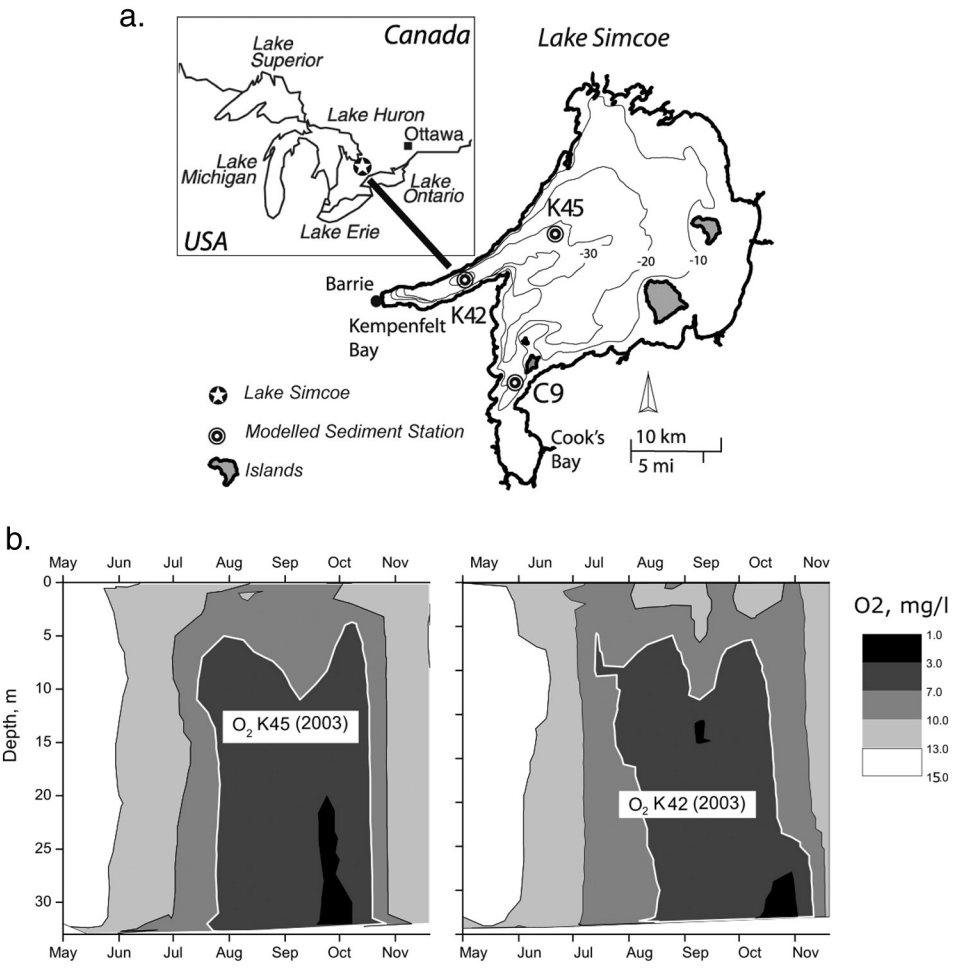

Fig. 1. (a) Monitoring stations in Lake Simcoe, Canada. (b) Seasonal vertical profiles of dissolved oxygen at stations K42 and K45.

the species concentration at the sediment–water interface. Settled organic matter (OM) is divided into degradable (X_{deg}) and refractory (X_{ref}) fractions (Chapra et al., 2015). The chemical composition of degradable OM is assumed to be equal to the Redfield stoichiometric ratio (Table S2). Other modeled solids include MnO_2, FeOOH, FeS, $CaCO_3$, $FeCO_3$, $MnCO_3$, and phosphorus binding forms as identified by *P* fractionation: loosely adsorbed (labile) *P* (extracted with NH_4Cl; NH_4Cl-TP), redox-sensitive bound *P* (extracted with bicarbonate dithionite, BD-TP), *P* bound to hydrated oxides of aluminum or iron oxides (extracted with NaOH, NaOH-SRP), organic bound *P* (extracted with NaOH, NaOH-NRP), carbonates bound *P* (apatite-*P*) (extracted with HCl, HCl-TP), and refractory *P* (Refract-*P*). The degradation rate constants of primary redox reactions for microbial decomposition of particulate labile OM with major oxidants are characterized by Monod kinetics with an inhibition term for less favorable electron acceptors (Tables S3 and S4). The modeled oxidants are oxygen, nitrate, manganese oxide, iron hydroxides, and sulfate (reactions PR1–5; Table S3). The oxidation of ammonium, sulfide, Fe-hydrooxides and Fe-sulfides are also considered as secondary redox reactions (reactions SR1–4; Table S3). The equilibrium processes are modeled as dynamic reactions with long relaxation-time constants to overcome numerical stability issues (Table S3). The model is solved numerically by integrating the system of partial differential equations in time, which are then discretized through a vertical grid of 180 layers within the 18 cm simulated core depth (Dittrich et al., 2009). Model specification was implemented using the open-source AQUASIM platform (Reichert, 1998). Model calibration was performed with the simplex (Nelder and Mead, 1965) and secant (Ralston and Jennrich, 1978) optimization methods, while the model simulations and their analysis were originally reported by McCulloch et al. (2013) and is also provided in Fig. S1. McCulloch et al. (2013) also presented a detailed identifiability analysis showing that most of the parameters can be reasonably constrained from the available data set, despite the complexity of the RTM structure (McCulloch et al., 2013).

Table 1
Limnological characteristics of the three study sites (K45, K42, and C9) in Lake Simcoe.

Station	K45	K42	C9
Maximal depth, m	39	42	21
TP[1] 2004–2008 (ice-free average), μg/L	13.8	14.7	14.8
Chl α[1], μg/L (±SD)	2.5 (±1.5)	2.8 (±1.6)	2.5 (±1.6)
Flux of OM[2] (J_{Corg}), annual average (2011), g DW/m^2/day	0.15	0.37	0.13
Age at 18 cm sediment core[3], years	188	104	70
Mineralization half-life period τ^{SWI} [4], years	2.45	0.55	2.31

[1] MOE (2010).
[2] McCulloch et al. (2013).
[3] Hiriart-Baer et al. (2011).
[4] Based on the present study

2.3. Sediment oxygen demand calculation

The SOD estimate accounts for O_2 fluxes associated with both OM mineralization and the oxidation of reduced substances in the sediments (Maerki et al., 2006; see also Tables 1 and 2 in McCulloch et al., 2013). The O_2 consumption rates in primary mineralization reactions were calculated by vertical integration of OM mineralization rates, expressed in O_2 equivalents (DiToro, 2001). The mineralization half-life period for degradable OM is estimated as $\tau = \frac{ln(2)}{r_{Xdeg}}$, where $r_{X\,deg}$ denotes a

total degradation rate (year^{-1}). The NH_4^+ fluxes were determined according to Fick's first law of diffusion based on centered difference formula approximated for discrete data (Li, 2011). The estimated fluxes were corrected for sediment tortuosity φ for fine-grained sediments (Eq. 4.120 in Boudreau, 1997):

$$J_{sed} = -\theta D_{sed}\frac{\partial NH4^+}{\partial z} \text{ where } D_{sed} = \frac{D_{diff}}{\varphi^2} = -\frac{D_{diff}}{\left(1-\ln\left(\theta^2\right)\right)}$$

where D_{diff} is a temperature-dependent free-solution diffusion coefficient (Yuan-Hui and Gregory, 1974; Dittrich et al., 2009). The SOD contribution to hypolimnetic DO depletion was quantified by integrating SOD daily rates over the entire summer stratification period and hypolimnetic area. The oxygen penetration depth is defined as the thickness of the oxic zone in the top layer of sediment cores (Cai and Sayles, 1996). In practice, we considered a threshold value of 2 μmol/L (~0.1 mg O_2/L; Li, 2011) as the detection limit of microelectrodes to delineate the boundary between oxic/anoxic zones.

2.4. Local sensitivity and analysis of scenarios

Local sensitivity analysis of simulated O_2 depth profiles and SOD estimates was based on the calculation of absolute-relative sensitivity functions $\delta^{ar}_{y,p}$ to eliminate the effect of different units of the examined parameters (Eq. 4.9c in Reichert, 1998).

$$\delta^{ar}_{y,p} = p\frac{\partial y}{\partial p_i} \approx p\frac{y(p_i+\Delta p_i)-y(p_i)}{\Delta p_i}$$

where y is the state variable (i.e., O_2 vertical profiles and SOD), p is the model parameter i, and Δp_i is equal to 1% of σ_{pi}, standard deviation of parameter p_i, which in turn was assigned an initial estimate of 10% of the calibration value. The sensitivity function $\delta^{ar}_{y,p}$ represents an absolute response of the state variable y_i to a certain percentage change of a parameter p_i under the assumption of linearity, and therefore $\delta^{ar}_{y,p}$ is approximated by the tangent of function $y(p_i)$ in p_i (see our Fig. 2a and Fig. 4.7 in Reichert, 1998). Small values of sensitivity function of a certain parameter imply low identifiability based on the available measurement data set.

The causal linkage between sediment diagenesis and lake trophic status was investigated with three scenarios (Table 2). The varying flux of OM (J_{Corg}) was used as a proxy for the lake's trophic changes. The impact of hypolimnetic DO concentrations on diagenetic redox reactions was examined through variations of the oxygen concentration at the sediment–water interface (O_2^{SWI}). The boundary conditions J_{Corg} and O_2^{SWI} were projected to the years 2020 and 2050 (Fig. 2b–d), with gradual annual changes in the lake's conditions. The first two scenarios considered average O_2^{SWI} and varying J_{Corg} ±20% relative to 2011 average conditions to illustrate our uncertainty about carbon flux estimates; a third scenario mimics the process of lake re-oligotrophication with lower J_{Corg} (−20%) and expected higher O_2^{SWI} (Table 2 and Fig. 2b–d). Based on McCulloch et al. (2013), the intra-annual dynamics of sedimentation fluxes have been defined with a piece-wise approach, postulating that the maximum flux of particulate matter occurs in summer and the minimum in winter (Fig. 2a–c). The boundary conditions for the O_2 concentrations at the SWI were also defined with a seasonal piece-wise approach, postulating that the maximum O_2 concentration occurs in the winter, when there is less consumption from the biota, and the minimum concentration in the summer, when the lake is stratified (Fig. 2a–c). All other boundary conditions remained intact from the 2011 sampling year (McCulloch et al., 2013). Outputs of local sensitivity analysis for model boundary conditions and major kinetic parameters were also used to calculate their correlation matrix, based on the open-source UNCSIM software package (Reichert, 2005). The software estimates variance–covariance matrix $\Sigma = s^2\,(D^TD)^{-1}$, where s^2 is error variance and D is the matrix of sensitivity functions (see

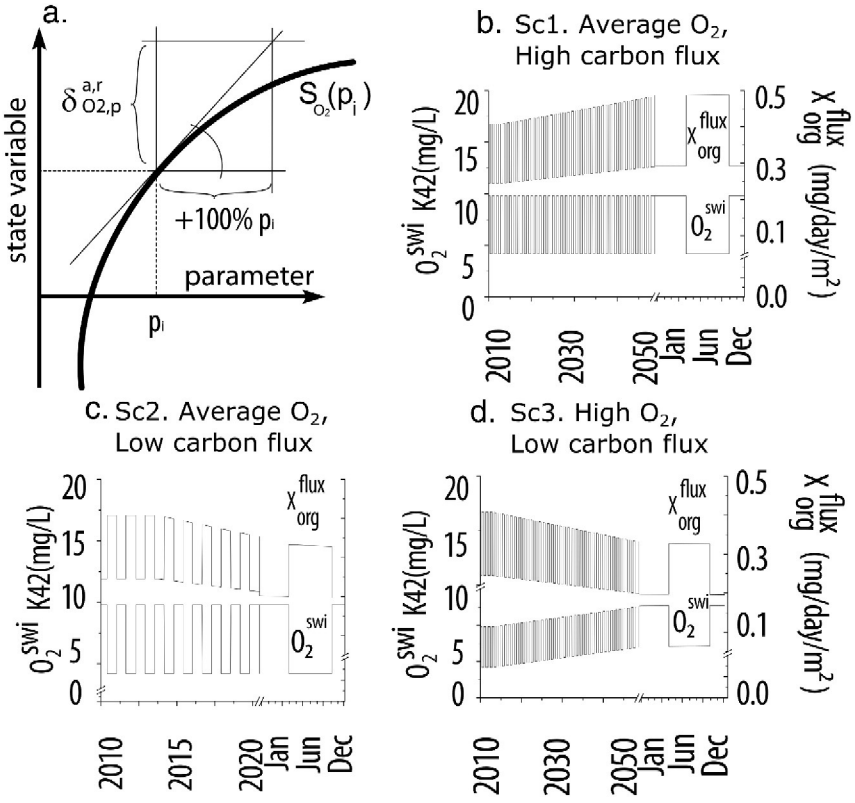

Fig. 2. (a) Conceptual schema of the absolute-relative sensitivity function, $\delta^{a,r}_{Variable,Parameter}$; (b–d) specification of the boundary conditions for the three scenarios examined with varying organic matter sedimentation fluxes (J_{Corg}) and deep oxygen concentration (O_2^{SWI}) at the study site K45.

Table 2
Scenarios of boundary conditions at sediment–water interface.

Scenarios/station	K45	K42	C9
1. Flux of OM, $J_{org,mean}$ (annual average), g DW m^{-2} day^{-1}	0.18	0.44	0.16
$O_2^{SWI}{}_{low}$ (summer), mg L^{-1}	3.7	2	3.7
2. Flux of OM, $J_{org,mean}$ (annual average), g DW m^{-2} day^{-1}	0.12	0.30	0.10
$O_2^{SWI}{}_{low}$ (summer), mg L^{-1}	3.7	2	3.7
3. Flux of OM, $J_{org,mean}$ (annual average), g DW m^{-2} day^{-1}	0.12	0.30	0.10
$O_2^{SWI}{}_{low}$ (summer), mg L^{-1}	7	7	7

Kuczera, 1990; Brun et al., 2001; Hill and Tiedeman, 2007) under the assumption of model linear response to parameters changes, parametric standard errors of 10% (McCulloch et al., 2013), and considering all other parameters fixed (see *ident* routine in UNCSIM manual at www.uncsim.eawag.ch).

3. Results

Local sensitivity analysis shows that pore water O_2 depth profiles are primarily dependent on the characterization of sediment porosity vertical variability (θ_{surf} and θ_{deep}) and the specification of dissolved oxygen concentrations at the sediment–water interface O_2^{SWI}, followed by the Monod kinetic parameters of aerobic microbial mineralization (k_{O2} and K_{O2}^{half}) (Fig. 3a and Table 3). The importance of O_2^{SWI} exponentially declines with the sediment depth, while the impact of porosity peaks close to the boundary of the oxic layer at 1 cm and gradually replaces the influence of O_2^{SWI}. Interestingly, the sensitivity values of the rate constant of Monod aerobic degradation (k_{O2}) and the associated half-saturation constant K_{O2}^{half} demonstrate mutual compensability, as suggested by the high correlation between the two parameters ($r_{k_{o2}\,,\,K_{O2}^{half}} = 0.97$, Table S5); that is, model output variations stemming from a change to one of the considered parameters can be compensated by an appropriate change to the other. The root mean square (RMS) values of sensitivity functions ($\delta_{O2,p}^{a,r}$) also identify the specification of the boundary conditions related to OM sedimentation flux rate (J_{Corg}) as another critical factor for reproducing pore water O_2 depth profiles (Table 3). In a similar manner, the refractory fraction in total OM flux (α_{Org_inert}) along with the fraction of total OM in total sediment flux (α_{Org}) were two particularly influential parameters to pore water O_2 depth profiles. Multiple studies have reported the importance of the diffusive boundary layer (DBL) on effective diffusivity, and thus the molecular diffusion in Fick's law is typically scaled by DBL thickness variability (Brand et al., 2009; O'Connor et al., 2009; Bryant et al., 2010). It should be noted, that DBL controls the actual oxygen concentration at SWI and therefore regulates the flux of oxygen from open water to the sediment surface over the laminar layer. While the presented diagenetic model postulates the simulation of solute fluxes under pre-defined boundary conditions at SWI, in reality the actual concentrations at SWI are modulated by transport processes across DBL. In a similar manner, our sensitivity analysis reinforces the notion that DBL thickness significantly impacts the flux of O_2, as the diffusion coefficient (D_{diff}) represents an intermediate sensitivity parameter that was ranked fifth in regard to its $\delta_{O2,p}^{a,r}$ value. Finally, calcite precipitation flux rate ($J_{CaCO3mean}$) was also included in the top ten most influential parameters, although its role is clearly less significant relative to the previously mentioned model inputs.

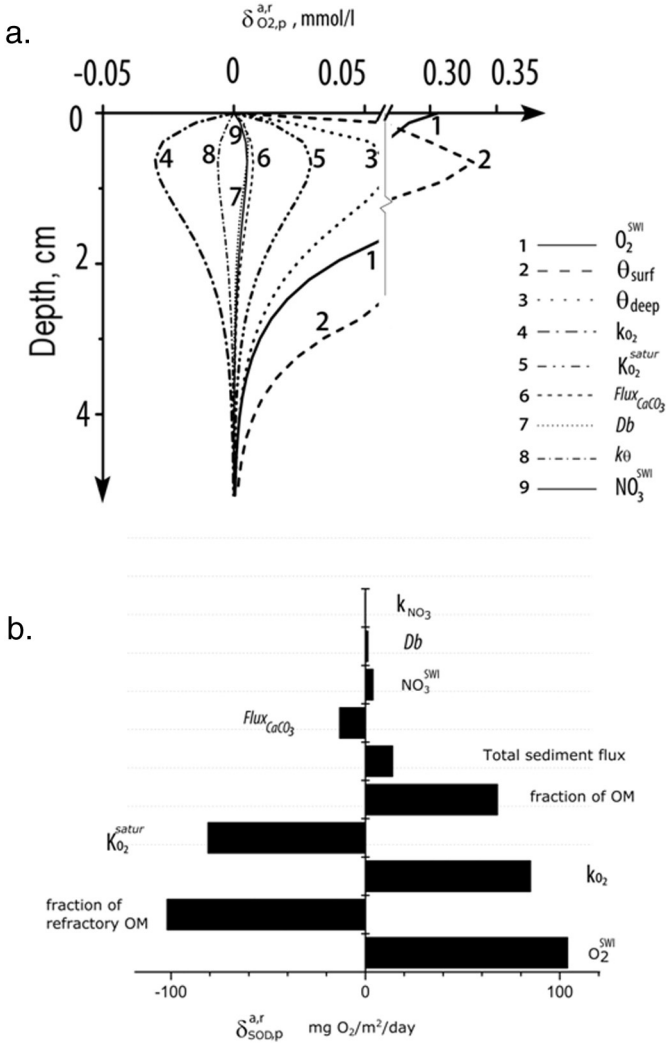

Fig. 3. (a) Vertical profiles of absolute-relative sensitivity functions for dissolved oxygen, $\delta_{O2,p}^{a,r}$. (b) Diagram of sensitivity functions for sediment oxygen demand, $\delta_{SOD,p}^{a,r}$.

Table 3
Local sensitivity analysis results for the state variables O_2 and SOD.

Ranking parameter		Root of mean squares* of sensitivity functions for O_2 (mmol l^{-1})
1	Porosity at the SWI	0.064
2	O_2^{SWI}	0.051
3	Refractory OM fraction in total OM flux	0.020
4	Fraction of total OM in total sediment flux	0.015
5	Diffusion coefficient for O_2 in sediment	0.015
6	OM flux	0.011
7	Porosity at 19.5 cm (core bottom)	0.011
8	Rate constant of OM degradation with oxygen (PR1)	0.007
9	Half-saturation constant for OM degradation with oxygen (PR1)	0.007
10	$CaCO_3$ flux	0.001

Ranking parameter		Absolute-relative sensitivity functions for SOD (mg O_2 m^{-2} day^{-1})
1	O_2^{SWI}	104.0
2	Refractory OM fraction in total OM flux	−103.0
3	Rate constant of OM degradation with oxygen (PR1)	85.0
4	Half-saturation constant for OM degradation with oxygen (PR1)	−81.0
5	Fraction of total OM in total sediment flux	68.0
6	Total sediment flux	14.0
7	$CaCO_3$ flux	−13.3
8	NO_3^{SWI}	4.0
9	Bioturbation coefficient	1.3
10	Rate constant of OM degradation with NO_3 (PR2)	−0.2

* RMS refers to $\sqrt{\frac{1}{n}(\sum_{i=1}^{n}\delta_{O_2\,i}^{a,r\,2})}$, where $\delta_{O_2}^{a,r}$ corresponds to the absolute-relative sensitivity function of oxygen, and i represents the vertical sediment layer.

Our analysis of scenarios suggests that the OPD in the sediments can profoundly respond to shifts in the boundary conditions, varying from 5.5 mm, under average O_2 conditions and high carbon fluxes, to 54 mm, under high O_2 conditions and low carbon fluxes (Fig. 4a, c). On a seasonal timescale, the OPD is also dynamic, increasing from 5.5 mm in the summer to 7.5 mm after the fall overturn with the first scenario (Fig. 4a). However, for a given O_2 regime at the sediment–water interface, our model also suggests that variations in the carbon fluxes do not induce significant OPD variability, i.e., 6.5 and 5.5 mm between Scenarios 1 and 2 (Fig. 4a, b). The dissolved *P* depth profiles are similarly characterized by pronounced seasonal variations (Fig. 4d–f). The model predicts a dynamic response to seasonally varying boundary conditions both in recent sediments within the top 5 cm (~last 25 years of deposition at station K42), but also in sediments deeper than 10 cm (~70 years of deposition). The elevated carbon flux rates with the first scenario compared to those examined with the second one led to an excessive TP accumulation in the upper sediment layer, which was manifested as a deepening by more than 2 cm of the TP-isopleth of 1.5 mg *P* g dry weight^{-1} (Fig. 4g, h). Further, the distinct differences of the sediment TP profiles between second and third scenarios, postulating similar organic fluxes but different oxygen variations at the sediment–water interface (Fig. 4h, i), reveal differences in *P* burial within the top sediment layer, as more deposited organic *P* mobilized to soluble phase under higher O_2^{SWI} levels (Fig. 4e, f). The latter pattern suggests greater influence of the aerobic processes on the sediment retention capacity, which is on par with the "decomposition hypothesis" of *P* release, suggesting that organic matter mineralization can be a major process of *P* release from the sediments (Hupfer and Lewandowski, 2008). Thus, the variability of iron and aluminum hydroxides may not always be the predominant factor that modulates pore water *P* mobilization or the fractions of labile and refractory material (Table 3).

Sensitivity functions that evaluate the impact of parameters associated with aerobic mineralization on SOD, $\delta_{SOD,p}^{a,r}$, highlight the importance of correct specification of O_2^{SWI} as well as the total (α_{Org}) and degradable fractions (α_{deg}) of depositing organic matter on the RTM-based SOD estimates (Fig. 3b and Table 3). The sensitivity analysis for SOD also highlights the compensatory effects between the rate constant of aerobic organic matter mineralization (k_{O2}) and the half-saturation constant (K_{O2}^{half}), 85 versus −81 mg O_2 m^{-2} day^{-1}, which highlights the identifiability issues underlying our SOD estimates. Given that the same parameters demonstrate weak correlation with model boundary conditions, such as O_2^{SWI} ($r_{k_{o2},\,O_2^{SWI}} = -0.002$; $r_{K_{o2},\,O_2^{SWI}} = -0.015$), α_{Org} ($r_{k_{o2},\,\alpha_{org}} = 0.001$; $r_{K_{o2},\,\alpha_{org}} = -0.106$), and α_{Org_inert} ($r_{k_{o2},\,\alpha_{org\_inert}} = -0.064$; $r_{K_{o2},\,\alpha_{org\_inert}} = -0.231$), it can be concluded that the derived SOD values are less dependent to the prior specification of individual boundary conditions at different sediment sites, but rather depict the collective outcome of all the pertinent sediment diagenesis mechanisms in a particular spatial location (Table 4). Based on the present conditions, the model registered substantial SOD differences among the three embayments (stations C9, K45, and K42) with annual average levels of 55, 168, and 802 mg O_2 m^{-2} day^{-1}, respectively. Variations of OM flux rates and (most importantly) dissolved oxygen O_2^{SWI} at the sediment–water interface can be translated to differences in SOD estimates of 700–800 mg O_2 m^{-2} day^{-1} prior to the thermal stratification onset at station K42 (Fig. 5). Interestingly, our model predicts comparable SOD values of 400 mg O_2 m^{-2} day^{-1} with the first two scenarios at the same location toward the end of the summer stratification, whereas high O_2^{SWI} values result in elevated SOD estimates, i.e., 1,300 mg O_2 m^{-2} day^{-1} (Fig. 5).

4. Discussion

4.1. Effects of boundary conditions on seasonal dynamics of O_2 depth profiles

Several recent studies have attempted to shed light on the causal connection between the sedimentation of autochthonous and allochthonous fluxes and OPD dynamics (Revsbech, 1989; Katsev et al., 2007; Li et al., 2012). In Lake Simcoe, both *in situ* measurements and

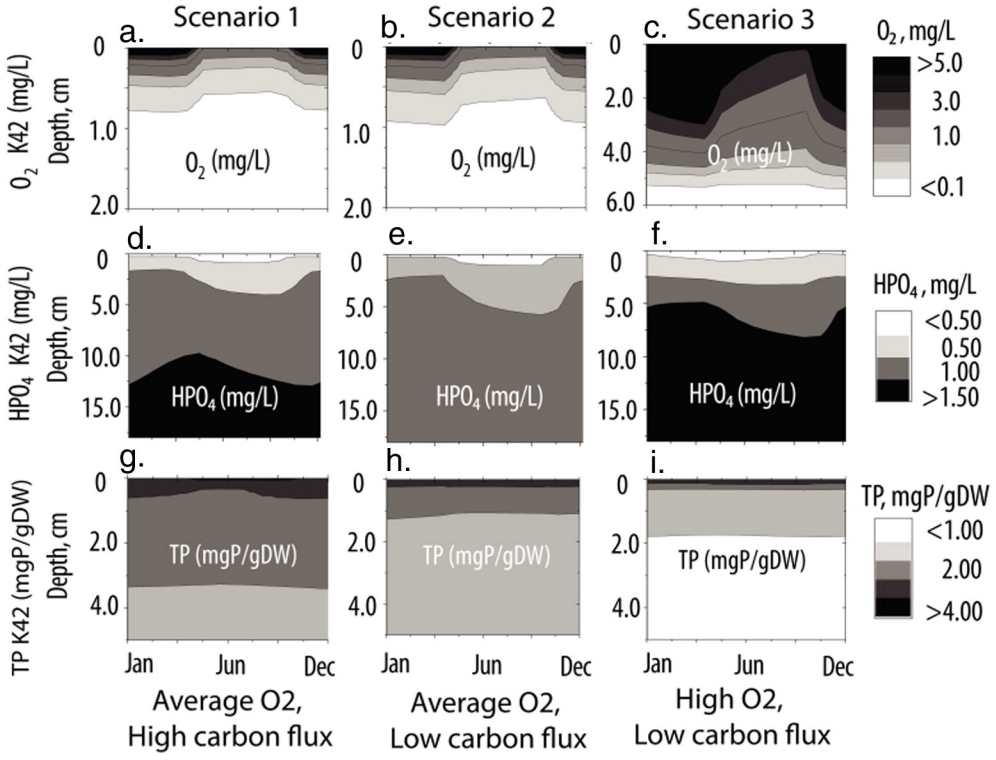

Fig. 4. Simulated vertical profiles of (a–c) dissolved oxygen, (d–f) soluble reactive phosphorus, and (g–i) total phosphorus in Kempenfelt Bay (site K42) under the three scenarios examined.

Table 4
Percentage contribution of the different pathways of oxygen consumption to the total SOD in different sediment layers (site K45).

Time scale*	SOD (%)	$r_{deg\ O2}$	r_{nitr}	$r_{oxy\ H2S}$	$r_{oxy\ FeS}$	r_{FeOOH}	F_{NH4}
		79.094%	0.001%	0.019%	4.181%	0.014%	16.691%
0–2 years	70.902%	69.530%	0.002%	0.010%	1.300%	0.060%	
2–5 years	9.025%	7.830%	0.001%	0.004%	1.190%	0.000%	
5–10 years	1.822%	1.200%	0.001%	0.001%	0.620%	0.000%	
>10 years	1.560%	0.480%	0.000%	0.000%	1.070%	0.010%	

* Time scale refers to sediment core dating from Hiriart-Baer et al. (2011). Pathways correspond to reaction rates related to oxygen consumption (see also Table S3).

model projections suggest that the seasonal variation of the carbon fluxes alone have limited impact on the seasonality of OPD dynamics

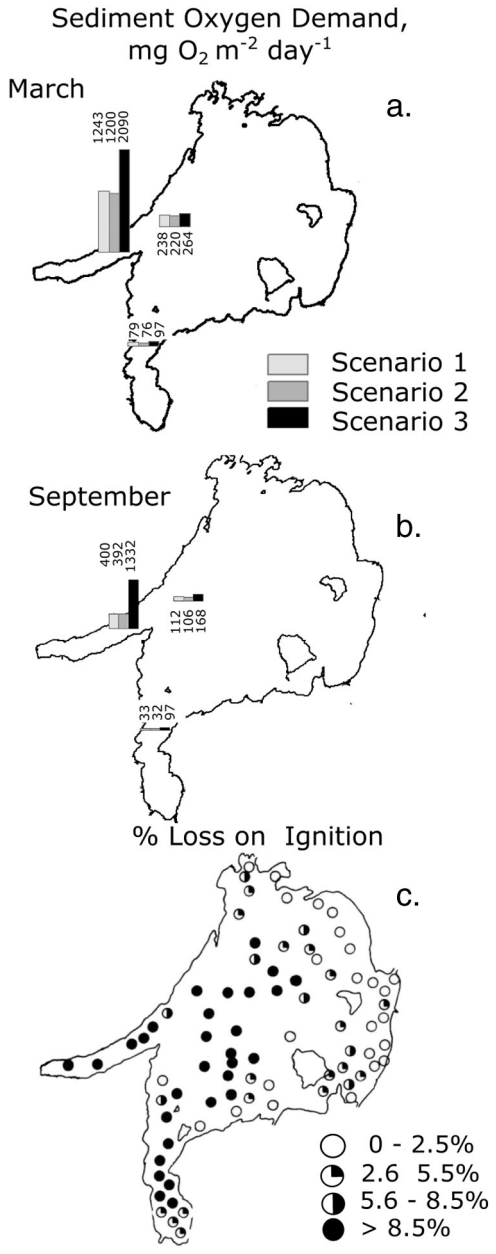

Fig. 5. Sediment oxygen demand in Lake Simcoe for March (a) and September (b), under the three scenarios examined. Panel (c) shows the historic spatial distribution of organic matter content in sediments based on a survey conducted by the MOE (1975). Samples were collected from 92 locations throughout the lake and analyzed for organic content, expressed as a percent weight loss on ignition (the weight difference before and after the dried sediment samples are exposed to 550 °C for 2 h in a furnace).

(Dittrich et al., 2013). By contrast, the comparison between two scenarios of similar OM fluxes (Scenarios 2 and 3) shows that the O_2^{SWI} increase from 3.7 to 7.0 mg L^{-1} can be accompanied by a tenfold OPD deepening from 5.5 to 53 mm. The OPD variability can profoundly affect the fluxes of redox-sensitive substances from the sediments (Cai and Sayles, 1996; Katsev et al., 2007; Li et al., 2012), and our result challenges the assumptions typically made to simulate early diagenesis processes. Specifically, models with simplified segmentation that assign fixed depths to oxic and anoxic layers with fixed porosity terms and coarse vertical resolution in deeper layers may fail to capture the seasonal range of sediment dynamics. Thus, our results call into question the practice of assigning temporally constant aerobic and anaerobic compartments and underscore the temporal variability of the aerobic zone as an essential feature of early diagenesis simulations in order to realistically depict fluxes of O_2 and reduced substances at the sediment–water column interface (Schauser et al., 2004; Müller et al., 2012).

In our modeling study, because of the lack of high-resolution data on the spatiotemporal sedimentation patterns, we opted for effective (temporally averaged) parameterization, such as the OM fraction in total settling fluxes and degradable fraction in total OM fluxes. Both parameters were shown to be particularly influential for reproducing the O_2 depth profiles (Table 3). Consistent with our findings, the sensitivity analysis studies by Katsev et al. (2007) and Schauser et al. (2004) highlighted the importance of accurately examining the qualitative and quantitative nature of particulate sedimentation rates. The OM fluxes in the hypolimnion of Lake Simcoe are modulated by both phytoplankton settling from the epilimnion and horizontal redistribution of OM from littoral to pelagic zones driven by resuspension (Gudimov et al., 2015). Importantly, the large fetch of Lake Simcoe and the fairly rapid hydrodynamic mixing may facilitate the localized impacts of the benthic processes in the littoral zone to shape ecosystem-scale patterns. Even though the omission of the latter mechanism has been shown to underestimate the sedimentation fluxes in lakes, little modeling work has been done to elucidate the importance of the coupling between inshore and offshore locations and evaluate its capacity to modulate lake biogeochemical cycling (Blais and Kalff, 1995; Meckler et al., 2004).

The ranking of the diffusion coefficient (D_{diff}), as a proxy of DBL, and the resultant oxygen surface concentration within the top 5 parameters in O_2 sensitivity function also emphasized the importance of the diffusive boundary layer (DBL) in the shallow sloping lakebed of Lake Simcoe. Similar findings were reported in the oligotrophic Lake Alpnach (Brand et al., 2009; Bryant et al., 2010; Scalo et al., 2013), where changes in DBL thickness from 0.25 to 1.5 mm diminished O_2 flux to the sediments from 0.24 to 0.15 g O_2 m^{-2} (Brand et al., 2009). In the latter modeling study, Brand et al. (2009) showed that the DBL governs the re-oxidation of Fe^{2+} and Mn^{2+} compounds, a finding that remains to be verified in Lake Simcoe. In the same context, it is interesting to note that the two lakes differ significantly with respect to their hydrodynamics, as Lake Alpnach is a seiche-driven alpine lake (Bryant et al., 2010), whereas the mixing processes in Lake Simcoe are governed by both geostrophic currents and internal waves (Bouffard and Boegman, 2011). Recent observations of benthic turbulence in Lake Simcoe showed that turbulent diffusivities in the benthic boundary layer are only intermittently high, following excursions of the thermocline in response to strong wind events (Cossu and Wells, 2013). Shear-driven convection is hypothesized to be a more important process for benthic turbulence levels than the breaking of non-linear internal waves at the level of thermocline (Cossu and Wells, 2013). However, more field data are needed to shed light on the interplay between hydrodynamic transport, DBL vertical distribution, and soluble component concentrations in Lake Simcoe.

4.2. Impact of hypolimnetic DO and organic matter quality on SOD estimates

High sensitivity of model parameters is a necessary condition for their identifiability during model calibration, in that parameters

demonstrating limited sensitivity response against model endpoints are the least identifiable from the provided data set. In a recent study by McCulloch et al. (2013), we showed that the consideration of *P*-binding forms along with the additional information typically collected from sediment cores (e.g., depth profiles of organic carbon, pH, porosity) act as adequate constraints during model calibration, thereby ensuring satisfactory identification of the calibration parameter vector. In particular, the parameters associated with the aerobic mineralization as a primary constituent of SOD were characterized by a collinearity index $\gamma = 10$, see parameter set (1e) in McCulloch et al.'s (2013) Table 6, suggesting low compensability problems among the calibrated process rates and thus satisfactory degree of confidence in the predicted SOD levels in Lake Simcoe.

The predicted SOD values are within the range typically reported for mesotrophic lakes in North America (Veenstra and Nolen, 1991; Smith and Matisoff, 2008) and correspond well with historical records of Lake Simcoe. The model estimated annual SOD of ~170 mg O_2 m^{-2} day^{-1} at station K45 lies within the range of 112 ± 226 mg O_2 m^{-2} day^{-1} reported by Snodgrass and Holubeshen (1992). However, the latter values should be treated with caution, as other empirical measurements averaged for Kempenfelt Bay and the main basin were indicative of SOD levels greater than 650 mg O_2 m^{-2} day^{-1} (MOE, 1975), which are also on par with our model estimates of ~800 mg O_2 m^{-2} day^{-1} at the Kempenfelt Bay mouth. The pronounced spatial differences of the SOD values between the two embayments and the offshore areas in Lake Simcoe are caused by the differences in primary productivity rates, the sedimentation fluxes that ultimately reach the sediment–water column interface, and the quality of the settled organic material (Hiriart-Baer et al., 2011). The SOD contribution to the hypolimnetic DO depletion in Lake Simcoe is estimated to be 23.7% and 12% in Kempenfelt Bay and the main basin, respectively, which is lower than a lake-wide estimate of 30% reported in the 1970s and 1980s (Snodgrass and Holubeshen, 1992). Given the considerable spatial variability in the sediment dynamics of Lake Simcoe, it is reasonable to infer that the uniform characterization of the early diagenesis processes in integrated water-sediment models is clearly inadequate (Gelda et al., 2012a; Smits and van Beek, 2013), and therefore additional mechanistic complexity may be required to accommodate the spatial patterns of settling fluxes and sediment reactivity rates (Meckler et al., 2004).

Our scenario analysis predicts significant seasonal SOD fluctuations in Kempenfelt Bay, station K42 ranging from 400 to 2100 mg O_2 m^{-2} day^{-1}, with the O_2^{SWI} acting as a major controlling factor relative to OM flux. The steep shore slopes and deep morphology of Kempenfelt Bay likely leads to enhanced hypolimnetic O_2 consumption (Blais and Kalff, 1995), and the deep hypolimnetic water are subsequently transported out of Kempenfelt Bay to the main basin (Baird & Associates, 2010). In laboratory experiments, the addition of DO to overlying water was found to cause similar SOD increases from 90 to 800 mg O_2 m^{-2} day^{-1} (Murrell and Lehrter, 2011). The SOD dependence on O_2^{SWI} boundary conditions in the mesotrophic Lake Simcoe is predominantly (≈80%) associated with the pathways of aerobic OM mineralization (Table 4). The flux of reduced species from sediment to the water column may constitute a substantial portion of oxygen sink, e.g., 70% in the hyper-eutrophic Lake Onondaga (Gelda et al., 1995). In Lake Simcoe, the modeled NH_4^+ flux accounts for ~17% in SOD, i.e., 0.48 mmol m^{-2} day^{-1} or 20 μmol m^{-2} hr^{-1}, which is below the reported levels of 1.91 ± 0.98 mmol m^{-2} day^{-1} for eutrophic lakes (Müller et al., 2012) but within the range of 10–30 μmol m^{-2} hr^{-1} reported for a mesotrophic lake in Denmark (Pelegrí and Blackburn, 1996). The SOD levels with high O_2^{SWI} were characterized by a 200–400% increase compared to those under lower O_2^{SWI} under the same OM deposition. This result can be explained by the enhanced aerobic organic matter mineralization when high O_2 conditions prevail in the sediment–water column interface. The latter finding is indicative of the need to distinguish between actual (limited by the available O_2 supplied to the sediments) and potential SOD (maximum oxygen demand with minimal inhibition by O_2 availability) in a lake (Bryant et al., 2010). The projected elevated SOD response under the re-oligotrophication scenario (high O_2 and low carbon fluxes) implies a feedback mechanism that can potentially delay the restoration of near-bottom oxygen levels even after nutrient loading reduction strategies come in effect.

As further validation, we compared the calibrated reactivity rates of organic matter against the range of sediment reactivity rates known to be associated with freshly settled phytoplankton (Fig. 6). The derived reactivity for all three monitoring stations is within uncertainty bounds of Middelburg's (1989) power model, as presented in Li et al. (2012), where the first-order reactivity term r_{deg} is expected to decrease exponentially with the sediment age and depth (Berner, 1980). Our diagenetic model demonstrates higher mineralization half-life periods, which are associated with overall lower reactivity rates in recent sediments for stations C9 and K45 (Table 1). Notably, the weakly negative slope of the K45 reactivity rate might suggest that the settled organic material in K45 experiences active mineralization in the water column, and therefore the fraction reaching the bottom is less reactive. Alternatively, the difference can be caused by structural limitations of Monod equations due to (i) identifiability issues between rate constants k_{O2} and half-saturation constant K_{O2}^{half}, which ultimately shape the slope of reactivity term, and (ii) assumption of depth-independent k_{O2} and K_{O2}^{half} values, unlike the age-dependent diagenetic parameters which offer more flexibility to capture variability of sediment reactivity with depth (Berg et al., 1998). On the other hand, the discrepancy in the half-life period at the C9 station relative to the other two study sites may reflect the increased terrestrial carbon export from the Holland Marsh agricultural watershed and/or the submerged aquatic macrophytes in shallow Cook's Bay (Dittrich et al., 2013). The macrophytes are characterized by 2–4 times higher half-life periods due to differences in cellulose, lignin, phenol compounds, and higher C:N:P ratios compared to phytoplankton (Meding and Jackson, 2003; Bianchini et al., 2008; Marinho et al., 2010). This observation is also consistent with the Hiriart-Baer et al's (2011) finding that higher C:N ratios characterize the sediments of K45 and C9 compared to Kempenfelt Bay (K42). It is also worth noting that the abundance of submerged aquatic macrophytes has tripled, from 1.2 to 3.1 kg m^{-2}, in Cook's Bay and at the offshore sites in Lake Simcoe from 1984 to 2008 (Ginn, 2011).

Our modeling study provides a convenient framework to track the contribution of sediments to SOD in Lake Simcoe. The mineralization of recent sediments (0–2 years) approximately represents 70% of SOD, whereas the older sediments (>5 years old) account for less than 4% of SOD, reflecting the gradual replacement of O_2 mineralization with

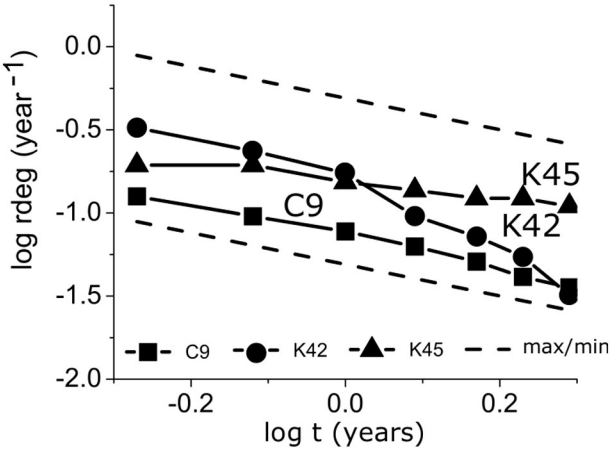

Fig. 6. Estimated sediment reactivity rates versus time for organic matter degradation against Middelburg's (1989) reactivity ranges (dashed lines) for freshly deposited marine sediments. The typical ranges of sediment reactivity rates were estimated by Li et al. (2012) based on Burdige's (2007) literature compilation of published analyses of sediment cores, lab experiments, and sediment traps.

FeS oxidation (Table 4). Importantly, the intermediate layer of 2–5 years is responsible for less than 10% of SOD, which suggests that SOD in Lake Simcoe will likely respond without a major time lag to an expected reduction in the OM deposition, should further exogenous *P* control is implemented (Matzinger et al., 2010). The same finding also implies that the OM mineralization in the water column remains a primary regulator of the hypolimnetic DO deficit (>75%). Similar conclusions were drawn from long-term hypolimnetic observations of artificially oxygenated Danish lakes, which reinforced the notion that the oxygen treatment should be accompanied by reduced nutrient inputs if permanent improvements of lake water quality are to be obtained (Liboriussen et al., 2009). Nonetheless, because of the presence of feedback mechanisms, we argue that short-term delays in the lake's response cannot be ruled out. For example, the projected elevated SOD response under the re-oligotrophication scenario (Fig. 2d) underscores the likelihood of a potential delay in the restoration of near-bottom oxygen levels even after nutrient-loading reduction strategies take place.

5. Conclusions

We used a reaction-transport diagenesis model to examine the interplay between deepwater oxygen levels and SOD in three basins of Lake Simcoe. Our modeling framework integrated biogeochemical and physical processes at the sediment–water interface and incorporated dynamic boundary conditions, such as OM sedimentation and O_2 concentration at the sediment–water interface, while rigorously assessing parameter sensitivity and model identifiability (McCulloch et al., 2013). The main findings of this study are as follows:

- ✓ Our model confirms previous empirical estimates of SOD in Lake Simcoe, suggesting that SOD contribution to overall hypolimnion DO deficit is less than 30%. Our model also predicts an order of magnitude difference in SOD levels between Kempenfelt Bay and Cook's Bay, which can be attributed to multiple factors, including the differences in primary production rates, the origins of the settling organic matter, redistribution of sediments and O_2^{SWI} due to differences in morphology and hydrodynamics.
- ✓ Porosity and oxygen concentration at the sediment–water interface are among the most important regulatory factors of the oxygen sediment profiles.
- ✓ Sediment oxygen uptake appears to be more sensitive to the oxygen concentrations at the sediment–water interface relative to the variability in organic matter sedimentation. In all scenarios, the rate of organic matter mineralization is limited by oxygen availability at the sediment–water column interface during the summer-stratified period. The relaxation of O_2 inhibition is the reason for the predicted increase in SOD levels during the fall turnover period after the mixing of the oxygen-saturated epilimnetic water masses with the hypolimnion. Our long-term model simulations also predict an increase of the OPD and total phosphorus depletion in the upper sediment layer following the establishment of conditions of low organic sedimentation flux and high DO concentrations in Lake Simcoe (re-oligotrophication scenario). The same scenario showed spatial SOD heterogeneity with highest levels observed at the Kempenfelt Bay, suggesting a feedback mechanism in the sediments that affects the oxygen concentration near the bottom of the lake. The significant spatial SOD variability underscores the importance of considering site-specific nutrient loading reduction targets, if we strive to achieve uniform improvements in deepwater oxygen concentrations in Lake Simcoe. The pace of the planned re-oligotrophication and the associated hypolimnetic DO improvement, induced by nutrient loading reductions, can be hindered over a short-term time scale due to the potential effects of a number of feedback mechanisms across sediment–water interface in Lake Simcoe. The increase in hypolimnetic DO can elevate the SOD and affect the near-bottom water quality, while the expected deepening of oxygen penetration depth can trigger aerobic mineralization of legacy organic matter which is currently residing in an anaerobic state.

Sediment diagenesis can be a significant driver of oxygen depletion in lakes and may dramatically impact hypolimnetic DO concentrations. The accurate depiction of the relevant mechanisms with mathematical models may offer an appealing methodology to overcome the inherent limitations of laboratory experiments, which cannot capture the broader implications of processes occurring in the sediment–water column interface. Our reactive-transport model represents a convenient framework to study diagenetic processes in time and space, and thus offers an essential management tool for addressing "what if?" questions related to the fate and transport of nutrients in the sediments. A logical next augmentation would be the integration of the sediment diagenesis processes with a water quality process-based model to dynamically examine the interplay among OM deposition, sediment dynamics, and dissolved oxygen patterns in both shallow and deepwaters. The adoption of a more holistic modeling tool will also be conceptually on par with the ecosystem management paradigm to restoring beneficial uses of impaired systems and will likely facilitate a multi-causal way of thinking that can more effectively accommodate ecosystem complexity (Zhang and Arhonditsis, 2008; Gudimov et al., 2012).

Several interesting lessons were learned from our study that pinpoint the challenges when integrating water column processes with sediment diagenesis dynamics in inland lakes, like Lake Simcoe: (i) Terrestrial subsidies represent an important source of carbon, and therefore may predominantly shape the spatial differences in organic matter loading and ultimately the variability in sediment reactivity. Furthermore, the senescence of aquatic emergent and submergent vegetation can significantly contribute to the organic matter sedimentation in lakes with extended littoral zones (Soetaert et al., 2000). (ii) The spatial variability of bioirrigation processes may also drive the differences in sediment degradation rates, which in turn may require consideration of site-specific information on bioturbation and bioirrigation activity (Michaud et al., 2010). In the same context, we should bear in mind that the establishment of dreissenid mussels in the Great Lakes area has strongly affected carbon deposition cycle from pelagic to littoral zones and also altered the richness of benthic communities. (iii) Correct representation of organic matter degradation in sediments invites further augmentation of traditional reactive-transport modeling frameworks, based on Monod-type kinetics with reaction rates and half-saturation constants. For example, recent sediment biogeochemical models introduced bioenergetics and thermodynamic properties of individual compounds in order to improve the representation of organic matter transformations (LaRowe and Van Cappellen, 2011). (iv) Recent advancements in the process characterization with water column models, such as consideration of time-variant C:N:P intracellular ratios in phytoplankton cells, phytoplankton succession patterns, depth-dependent bacterial mineralization, are essential steps to improve the fidelity of simulations of deposition fluxes (Meckler et al., 2004).

Acknowledgments

This project was undertaken with the financial support of the Government of Canada, provided through the Department of the Environment (Lake Simcoe Clean-Up Fund) and the University of Toronto (Start-Up Funds to Maria Dittrich). Funding for this study was provided by the National Sciences and Engineering Research Council of Canada (NSERC) through a Doctoral Graduate Scholarship (Alex Gudimov) and two Discovery Grants (George Arhonditsis and Maria Dittrich).

Appendix A. Supplementary data

Supplementary data to this article can be found online at http://dx.doi.org/10.1016/j.ecoinf.2015.11.005.

References

Annadotter, H., Cronberg, G., Aagren, R., Lundstedt, B., Nilsson, P.-Å., Ströbeck, S., 1999. Multiple Techniques for Lake Restoration, in The Ecological Bases for Lake and Reservoir Management. Springer, Neverlands, pp. 77–85.

Baird & Associates, 2010. 3D Hydrodynamic Modelling of Flushing Rates in Lake Simcoe Bays. Report to Lake Simcoe Region Conservation Authority.

Berg, P., Risgaard-Petersen, N., Rysgaard, S., 1998. Interpretation of measured concentration profiles in sediment pore water. Limnol. Oceanogr. 43, 1500–1510.

Berner, R.A., 1980. Early diagenesis: a theoretical approach. Princeton University Press (241 p).

Bianchini Jr., I., Cunha-Santino, M., Peret, A., 2008. Oxygen demand during mineralization of aquatic macrophytes from an oxbow lake. Braz. J. Biol. 68, 61–67.

Blais, J.M., Kalff, J., 1995. The influence of lake morphometry on sediment focusing. Limnol. Oceanogr. 40, 582–588.

Boudreau, B.P., 1997. Diagenetic models and their implementation. Springer, New York (417p).

Bouffard, D., Boegman, L., 2011. Spatio-temporal dynamics of the basin scale internal waves in Lake Simcoe. Proceedings 7th Int Symp on Stratified Flows, Rome, Italy (August 22 - 26, 2011, 6 pp.).

Brand, A., Dinkel, C., Wehrli, B., 2009. Influence of the diffusive boundary layer on solute dynamics in the sediments of a seiche-driven lake: A model study. J Geophys Res-Biogeo (2005-2012), 114(1), art. no. G01010.

Brun, R., Reichert, P., Künsch, H.R., 2001. Practical identifiability analysis of large environmental simulation models. Water Resour. Res. 37 (4), 1015–1030.

Bryant, L.D., Lorrai, C., McGinnis, D., Brand, A., Wüest, A., Little, J.C., 2010. Variable sediment oxygen uptake in response to dynamic forcing. Limnol. Oceanogr. 55, 950–964.

Burdige, D.J., 2007. Preservation of organic matter in marine sediments: controls, mechanisms, and an imbalance in sediment organic carbon budgets? Chem. Rev. 107, 467–485.

Cai, W.J., Sayles, F.L., 1996. Oxygen penetration depths and fluxes in marine sediments. Mar. Chem. 52, 123–131.

Carignan, R., Lean, D.R.S., 1991. Regeneration of dissolved substances in a seasonally anoxic lake: the relative importance of processes occurring in the water column and in the sediments. Limnol. Oceanogr. 36, 683–707.

Chapra, S.C., Gawde, R.K., Auer, M.T., Gelda, R.K., Urban, N.R., 2015. Sed2K: modeling Lake Sediment Diagenesis in a Management Context. J. Environ. Eng. 141.

Charlton, M.N., Milne, J.E., Booth, W.G., Chiocchio, F., 1993. Lake Erie offshore in 1990: restoration and resilience in the central basin. J. Great Lakes Res. 19, 291–309.

Cossu, R., Wells, M.G., 2013. The interaction of large amplitude internal seiches with a shallow sloping lakebed: observations of benthic turbulence in Lake Simcoe, Ontario, Canada. PLoS ONE 8 (3), e57444. http://dx.doi.org/10.1371/journal.pone.0057444.

DiToro, D.M., 2001. Sediment flux modeling Vol. 116. Wiley-Interscience, New York (624 pp.).

Dittrich, M., Wehrli, B., Reichert, P., 2009. Lake sediments during the transient eutrophication period: reactive-transport model and identifiability study. Ecol. Model. 220, 2751–2769.

Dittrich, M., Chesnyuk, A., Gudimov, A., McCulloch, J., Quaizi, S., Young, J., Winter, J., Stainsby, E., Arhonditsis, G., 2013. Phosphorus retention in a mesotrophic lake under transient loading conditions: insights from a sediment phosphorus binding form study. Water Res. 47, 1433–1447.

Eimers, M.C., Winter, J.G., Scheider, W.A., Watmough, S.A., Nicholls, K.H., 2005. Recent changes and patterns in the water chemistry of Lake Simcoe. J. Great Lakes Res. 31, 322–332.

Evans, D.O., 2007. Effects of hypoxia on scope-for-activity and power capacity of lake trout (*Salvelinus namaycush*). Can. J. Fish. Aquat. Sci. 64 (2), 345–361.

Gächter, R., Wehrli, B., 1998. Ten years of artificial mixing and oxygenation: no effect on the internal phosphorus loading of two eutrophic lakes. Environ. Sci. Technol. 32, 3659–3665.

Gelda, R.K., Auer, M.T., Effler, S.W., 1995. Determination of sediment oxygen demand by direct measurement and by inference from reduced species accumulation. Mar. Freshw. Res. 46, 81–88.

Gelda, R.K., Effler, S.W., Matthews, D.A., Owens, E.M., Hurteau, C.A., Chapra, S.C., Auer, M.T., Gawde, R.K., 2012a. Calibration and application of a sediment accumulation rate model–a case study. Inland Waters 2, 23–36.

Gelda, R.K., Owens, E.M., Matthews, D.A., Effler, S.W., Chapra, S.C., Auer, M.T., Gawde, R.K., 2012b. Modeling effects of sediment diagenesis on recovery of hypolimnetic oxygen. J. Environ. Eng. 139, 44–53.

Ginn, B.K., 2011. Distribution and limnological drivers of submerged aquatic plant communities in Lake Simcoe (Ontario, Canada): utility of macrophytes as bioindicators of lake trophic status. J. Great Lakes Res. 37, 83–89.

Gudimov, A., O'Connor, E., Dittrich, M., Jarjanazi, H., Palmer, M.E., Stainsby, E.A., Winter, J.G., Young, J.D., Arhonditsis, G.B., 2012. Continuous Bayesian network for studying the causal links between phosphorus loading and plankton patterns in Lake Simcoe, Ontario, Canada. Environ. Sci. Technol. 46 (13), 7283–7292.

Gudimov, A., Kim, D.K., Young, J.D., Palmer, M.E., Dittrich, M., Winter, J.G., Stainsby, E., Arhonditsis, G.B., 2015. Examination of the role of dreissenids and macrophytes in the phosphorus dynamics of Lake Simcoe, Ontario, Canada. Ecol. Inform. 26 (3), 36–53. http://dx.doi.org/10.1016/j.ecoinf.2014.11.007.

Hill, M., Tiedeman, C., 2007. Effective calibration of groundwater models, with analysis of data, sensitivities, predictions, and uncertainty. John Wiely, NY, p. 455.

Hiriart-Baer, V.P., Milne, J.E., Marvin, C.H., 2011. Temporal trends in phosphorus and lacustrine productivity in Lake Simcoe inferred from lake sediment. J. Great Lakes Res. 37, 764–771.

Hupfer, M., Lewandowski, J., 2008. Oxygen controls the phosphorus release from lake sediments—a long-lasting paradigm in limnology. Int. Rev. Hydrobiol. 93 (4-5), 415–432.

Katsev, S., Chaillou, G., Sundby, B., Mucci, A., 2007. Effects of progressive oxygen depletion on sediment diagenesis and fluxes: a model for the lower St. Lawrence River Estuary. Limnol. Oceanogr. 52, 2555–2568.

Kim, D.K., Zhang, W., Rao, Y.R., Watson, S., Mugalingam, S., Labencki, T., Dittrich, M., Morley, A., Arhonditsis, G.B., 2013. Improving the representation of internal nutrient recycling with phosphorus mass balance models: a case study in the Bay of Quinte, Ontario, Canada. Ecol. Model. 256, 53–68.

Kuczera, G., 1990. Assessing hydrologic model nonlinearity using response surface plots. J. Hydrol. 118 (1), 143–161.

LaRowe, D.E., Van Cappellen, P., 2011. Degradation of natural organic matter: a thermodynamic analysis. Geochim. Cosmochim. Acta 75-8, 2030–2042.

Li, J., 2011. Diagenesis and sediment–water exchanges in organic-poor sediments of Lake Superior Master's Thesis The University of Minnesota.

Li, J., Crowe, S.A., Miklesh, D., Kistner, M., Canfield, D.E., Katsev, S., 2012. Carbon mineralization and oxygen dynamics in sediments with deep oxygen penetration, Lake Superior. Limnol. Oceanogr. 57, 1634.

Liboriussen, L., Søndergaard, M., Jeppesen, E., Thorsgaard, I., Grünfeld, S., Jakobsen, T.S., Hansen, K., 2009. Effects of hypolimnetic oxygenation on water quality: results from five Danish lakes. Hydrobiologia 625, 157–172.

Maerki, M., Müller, B., Wehrli, B., 2006. Microscale mineralization pathways in surface sediments: a chemical sensor study in Lake Baikal. Limnol. Oceanogr. 51, 1342–1354.

Marinho, C.C., Meirelles-Pereira, F., Gripp, Ad.R, Guimarães, Cd.C., Esteves, Fd.A., Bozelli, R.L., 2010. Aquatic macrophytes drive sediment stoichiometry and the suspended particulate organic carbon composition of a tropical coastal lagoon. Acta Limnologica Brasiliensia 22, 208–217.

Matthews, D.A., Effler, S.W., 2006. Long-term changes in the areal hypolimnetic oxygen deficit (AHOD) of Onondaga Lake: evidence of sediment feedback. Limnol. Oceanogr. 51, 702–714.

Matzinger, A., Müller, B., Niederhauser, P., Schmid, M., Wüest, A., 2010. Hypolimnetic oxygen consumption by sediment–based reduced substances in former eutrophic lakes. Limnol. Oceanogr. 55, 2073–2084.

McCulloch, J., Gudimov, A., Arhonditsis, G., Chesnyuk, A., Dittrich, M., 2013. Dynamics of P-binding forms in sediments of a mesotrophic hard-water lake: insights from non-steady state reactive-transport modeling, sensitivity and identifiability analysis. Chem. Geol. 354, 216–232.

Meckler, A., Schubert, C., Cowie, G., Peiffer, S., Dittrich, M., 2004. New organic matter degradation proxies: valid in lake systems? Limnol. Oceanogr. 49, 2023–2033.

Meding, M.E., Jackson, L.J., 2003. Biotic, chemical, and morphometric factors contributing to winter anoxia in prairie lakes. Limnol. Oceanogr. 48, 1633–1642.

Michaud, E., Robert, C.A., Stora, G., 2010. Sedimentary organic matter distributions, burrowing activity, and biogeochemical cycling: natural patterns and experimental artifacts. Estuar. Coast. Shelf Sci. 90–1, 21–34.

Middelburg, J.J., 1989. A simple rate model for organic matter decomposition in marine sediments. Geochim. Cosmochim. Acta 53, 1577–1581.

MOE, 1975. Ontario Ministry of the Environment. Lake Simcoe basin. A Water Quality and Use Study. Queen's Printer for Ontario.

MOE, 2010. Ontairo Ministry of the Environment. Lake Simcoe Water Quality Update. Queen's Printer for Ontario, Toronto, Ont (Available from http://www.lsrca.on.ca/about/ annual_report.php).

Mueller, R., Stadelmann, P., 2004. Fish habitat requirements as the basis for rehabilitation of eutrophic lakes by oxygenation. Fish. Manag. Ecol. 11, 251–260.

Müller, B., Bryant, L.D., Matzinger, A., Wüest, A., 2012. Hypolimnetic oxygen depletion in eutrophic lakes. Environ. Sci. Technol. 46, 9964–9971.

Murrell, M.C., Lehrter, J.C., 2011. Sediment and lower water column oxygen consumption in the seasonally hypoxic region of the Louisiana continental shelf. Estuar. Coasts 34, 912–924.

Nelder, J.A., Mead, R., 1965. A simplex method for function minimization. Comput. J. 7 (4), 308–313.

North, R.L., 2013. The state of Lake Simcoe (Ontario, Canada): the effects of multiple stressors on phosphorus and oxygen dynamics. Inland Waters 3, 51–74.

O'Connor, B.L., Hondzo, M., Harvey, J.W., 2009. Incorporating both physical and kinetic limitations in quantifying dissolved oxygen flux to aquatic sediments. J. Environ. Eng. 135 (12), 1304–1314.

Paraska, D.W., Hipsey, M.R., Salmon, S.U., 2014. Sediment diagenesis models: review of approaches, challenges and opportunities. Environ. Model Softw. 61, 297–325.

Pelegrí, S.P., Blackburn, T.H., 1996. Nitrogen cycling in lake sediments bioturbated by *Chironomus plumosus* larvae, under different degrees of oxygenation. Hydrobiologia 325, 231–238.

Ralston, M.L., Jennrich, R.I., 1978. DUD, A derivative-free algorithm for nonlinear least squares. Technometrics 20, 7–14.

Reichert, P., 1998. AQUASIM 2.0 computer program for the identification and simulation of aquatic systems. User Manual. EAWAG report (ISBN 3-906484-19-5).

Reichert, P., 2005. UNCSIM a computer programme for statistical inference and sensitivity, identifiability, and uncertainty analysis Retrieved at www.uncsim.eawag.ch/references/ reichert_2005_uncsim.pdf.

Revsbech, N.P., 1989. An oxygen microsensor with a guard cathode. Limnol. Oceanogr. 34, 474–478.

Scalo, C., Boegman, L., Piomelli, U., 2013. Large-eddy simulation and low-order modeling of sediment-oxygen uptake in a transitional oscillatory flow. J. Geophys. Res. Oceans 118, 1926–1939.

Schauser, I., Hupfer, M., Brüggemann, R., 2004. SPIEL—a model for phosphorus diagenesis and its application to lake restoration. Ecol. Model. 176, 389–407.

Smith, D.A., Matisoff, G., 2008. Sediment oxygen demand in the central basin of Lake Erie. J. Great Lakes Res. 34, 731–744.

Smits, J.G.C., van Beek, J.K.L., 2013. ECO: a generic eutrophication model including comprehensive sediment–water interaction. PLoS ONE 8, e68104.

Snodgrass, W.J., Holubeshen, J., 1992. Estimation of phosphorus loadings and evaluation of empirical oxygen models for Lake Simcoe for 1970–1990. LSEMS Implementation Tech. Rep. Imp. B. 15.
Soetaert, K., Middelburg, J.J., Herman, P.M., Buis, K., 2000. On the coupling of benthic and pelagic biogeochemical models. Earth Sci. Rev. 51-1, 173–201.
Veenstra, J.N., Nolen, S.L., 1991. In-Situ sediment oxygen demand in five Southwestern U.S. lakes. Water Res. 25, 351–354.
Wetzel, R.G., 2001. Limnology, Lake and River Ecosystems. Academic Press, USA (1006 pp.).
Wu, R.S., Zhou, B.S., Randall, D.J., Woo, N.Y., Lam, P.K., 2003. Aquatic hypoxia is an endocrine disruptor and impairs fish reproduction. Environ. Sci. Technol. 37 (6), 1137–1141.
Young, J.D., Winter, J.G., Molot, L., 2011. A re-evaluation of the empirical relationships connecting dissolved oxygen and phosphorus loading after dreissenid mussel invasion in Lake Simcoe. J. Great Lakes Res. 37, 7–14.
Yuan-Hui, L., Gregory, S., 1974. Diffusion of ions in sea water and in deep-sea sediments. Geochim. Cosmochim. Acta 38 (5), 703–714.
Zhang, W., Arhonditsis, G.B., 2008. Predicting the frequency of water quality standard violations using Bayesian calibration of eutrophication models. J. Great Lakes Res. 34, 698–720.

MODELING THE INTERPLAY BETWEEN DEEP WATER OXYGEN DYNAMICS AND SEDIMENT DIAGENESIS IN A HARD-WATER MESOTROPHIC LAKE

(SUPPORTING INFORMATION)

Alex Gudimov, Jalene McCulloch, Jianwen Chen, Phoung Dong,

George Arhonditsis, Maria Dittrich*

Department of Physical and Environmental Sciences, University of Toronto Scarborough
1265 Military Trail, Toronto, M1C 1A4, Canada

* Corresponding author
Tel. +1 416 208 2786, Fax. +1 416 287 7279, e-mail: mdittrich@utsc.utoronto.ca

Figure S1. Comparison between observed and modeled vertical sediment profiles for *pH*, oxygen, and porosity. Figure adapted from McCulloch et al. (2013).

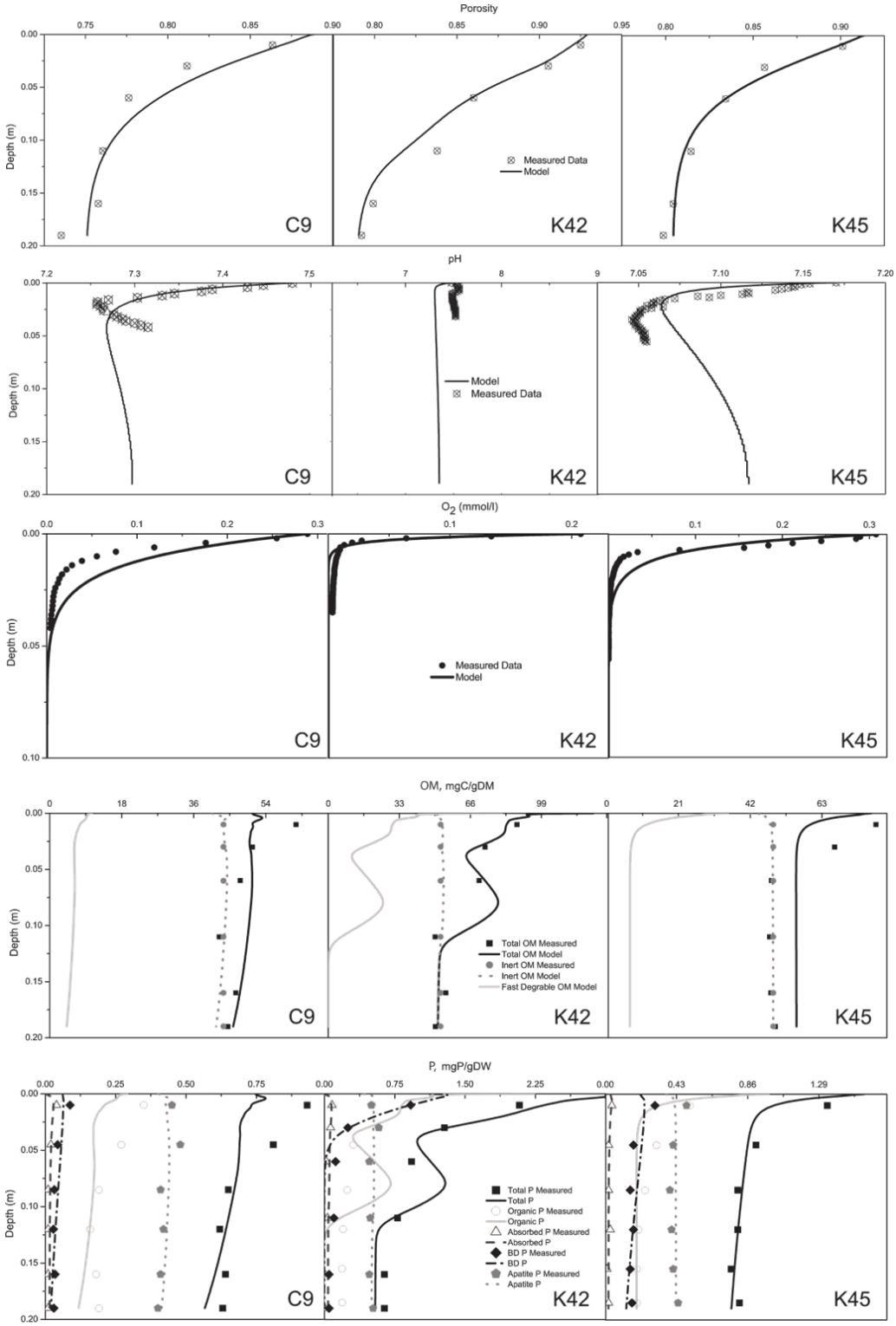

Table S1. Diagenetic reactions in the model. X_{org} indicates organic matter with the composition presented in Table 2-SI. Table adapted from McCulloch et al. (2013)

	Rates	Reactants	Products
Primary redox reduction	PR1	$X_{org} + O_2 + H_2O$	$NH_4^+ + HPO_4^- + HCO_3^- + H^+ + HS^-$
	PR2	$X_{org} + NO_3^- + H_2O$	$NH_4^+ + HPO_4^- + HCO_3^- + H^+ + HS^- + N_2$
	PR3	$X_{org} + X_{MnO2} + H^+$	$NH_4^+ + HPO_4^- + HCO_3^- + HS^- + H_2O + Mn^{2+}$
	PR4	$X_{org} + X_{FeOOH} + H^+$	$NH_4^+ + HPO_4^- + HCO_3^- + H^+ + HS^- + H_2O + Fe^{2+}$
			$NH_4^+ + HPO_4^- + HCO_3^- + H^+ + HS^-$
	PR5	$X_{org} + SO_4^{2-} + H_2O$	
Secondary redox reaction	SR1	$NH_4^+ + 2O_2$	$NO_3^- + 2H^+ + H_2O$
	SR2	$H_2S + 2O_2$	$SO_4^{2-} + 2H^+$
	SR3	$8X_{FeOOH} + H_2S + 14H^+$	$8Fe^{2+} + SO_4^{2-} + 12H_2O$
	SR4	$FeS + 2O_2$	$Fe^{2+} + SO_4^{2-}$
Mineral precipitation-dissolution reactions	MR1	$Mn^{2+} + HCO_3^-$	$X_{MnCO3} + H^+$
	MR2	$Ca^{2+} + HCO_3^-$	$X_{CaCO3} + H^+$
	MR3	$Fe^{2+} + CO_3^{2-}$	$2X_{FeCO3}$
	MR4	$Fe^{2+} + HS^-$	$X_{FeS} + H^+$
Acid base equilibrium conditions	ER1	H_2O	$H^+ + OH^-$
	ER2	$H_2CO_3^*$	$HCO_3^- + H^+$
	ER3	HCO_3^-	$CO_3^{2-} + H^+$
	ER4	NH_4^+	$NH_3 + H^+$
	ER5	$H_2PO_4^{2-}$	$HPO_4^- + H^+$
	ER6	H_2S	$HS^- + H^+$
	ER7	HS^-	$S^{2-} + H^+$
Phosphorus Binding Forms Reactions	PBR1	HPO_4^-	$X_{Absorbed\_P}$
	PBR2	$3Ca^{2+} + 2HPO_4^{2-}$	$X_{Apatite\_P} + 4H^+$
	PBR3	$4Fe^{2+} + 4HPO_4^{2-} + 8HCO_3^- + O_2$ X_{Fe_P}	$4X_{Fe\_P} + 8CO_2 + 4X_{FeOOH}$
	PBR4	HPO_4^-	$Fe^{2+} + HPO_4^-$
	PBR5		X_{Al_P}

Table S2. Stoichiometric coefficients for organic matter. Table adapted from McCulloch et al. (2013).

Composition of Organic Components	Atoms	Mass fraction
α_C	106	0.358 g C/g OM
α_H	263	0.074 g H/g OM
α_O	110	0.496 g O/g OM
α_N	16	0.063 g N/g OM
α_P	1	0.009 g P/g OM
α_S	0	0.000 g S/g OM
Total Redfield composition[1]	3550	1 g OM/g OM

[1)] Dittrich et al. (2009)

Table S3. Reactions rates in the model. S_i and X_i represent the dissolved and particulate phase concentrations of a substance *i*. Table adapted from McCulloch et al. (2013).

Primary redox reactions[1], r_{deg_i}

$$PR2 = k_{NO3} \frac{K_{O2}^{satur}}{K_{O2}^{satur} + S_{O2}} \frac{S_{NO3}}{K_{NO3}^{satur} + S_{NO3}} X_{org}$$

$$PR3 = k_{MnO2} \frac{K_{O2}^{satur}}{K_{O2}^{satur} + S_{O2}} \frac{K_{NO3}^{satur}}{K_{NO3}^{satur} + S_{NO3}} \frac{X_{MnO2}}{K_{MnO2}^{satur} + X_{MnO2}} X_{org}$$

$$PR4 = k_{FeOOH} \frac{K_{O2}^{satur}}{K_{O2}^{satur} + S_{O2}} \frac{K_{NO3}^{satur}}{K_{NO3}^{satur} + S_{NO3}} \frac{K_{MnO2}^{satur}}{K_{MnO2}^{satur} + X_{MnO2}} \frac{X_{FeOOH}}{K_{FeOH}^{satur} + X_{FeOH}} X_{org}$$

$$PR5 = k_{SO4} \frac{K_{O2}}{K_{O2} + S_{O2}} \frac{K_{NO3}}{K_{NO3} + S_{NO3}} \frac{K_{MnO2}}{K_{MnO2} + S_{MnO2}} \frac{X_{FeOOH}}{K_{FeOOH} + S_{FeOOH}} \frac{S_{SO4}}{K_{SO4} + S_{SO4}} X_{orgfast}$$

Secondary redox reactions

$$SR1 = k_{nitri} \frac{S_{NH4}}{K_{nitriNH4}^{satur} + S_{NH4}} \frac{S_{O2}}{K_{nitriO2}^{satur} + S_{O2}}$$

$$SR2 = k_{oxiHS} S_{HS} S_{O2}$$

$$SR3 = k_{FeOOHS} X_{FeOOH} S_{HS}$$

$$SR4 = k_{FeSO} X_{FeS} S_{O2}$$

Mineral precipitation-dissolution reactions

$$MR1 = \begin{cases} k_{eq\ MnCO3\ prec} \left(\frac{S_{Mn} S_{CO3}}{K_{eq\ MnCO3}} - 1 \right) & \text{if } \frac{S_{Mn} S_{CO3}}{K_{eq\ MnCO3}} > 1 \\ k_{eq\ MnCO3\ diss} \left(\frac{S_{Mn} S_{CO3}}{K_{eq\ MnCO3}} - 1 \right) X_{FeS} & \text{if } \frac{S_{Mn} S_{CO3}}{K_{eq\ MnCO3}} < 1 \end{cases}$$

$$MR3 = \begin{cases} k_{eq\ FeCO3\ prec} \left(\frac{S_{Fe} S_{CO3}}{K_{eq\ CaCO3}} - 1 \right) & \text{if } \frac{S_{Fe} S_{CO3}}{K_{eq\ FeCO3}} > 1 \\ k_{eq\ FeCO3\ diss} \left(\frac{S_{Fe} S_{CO3}}{K_{eq\ FeCO3}} - 1 \right) X_{FeCO3} & \text{if } \frac{S_{Fe} S_{CO3}}{K_{eq\ FeCO3}} < 1 \end{cases}$$

$$MR2 = \begin{cases} k_{eq\ CaCO3\ prec} \left(\frac{S_{Ca} S_{CO3}}{K_{eq\ CaCO3}} - 1 \right) & \text{if } \frac{S_{Ca} S_{CO3}}{K_{eq\ CaCO3}} > 1 \\ k_{eq\ CaCO3\ diss} \left(\frac{S_{Ca} S_{CO3}}{K_{eq\ CaCO3}} - 1 \right) X_{CaCO3} & \text{if } \frac{S_{Ca} S_{CO3}}{K_{eq\ CaCO3}} < 1 \end{cases}$$

$$MR4 = \begin{cases} k_{eq,FeS,prec} \left(\frac{S_{Fe} S_{S2}}{K_{eq,FeS}} - 1 \right) & \text{if } \frac{S_{Fe} S_{S2}}{K_{eq,FeS}} > 1 \\ k_{eq,FeS,diss} \left(\frac{S_{Fe} S_{S2}}{K_{eq,FeS}} - 1 \right) X_{FeS} & \text{if } \frac{S_{Fe} S_{S2}}{K_{eq,FeS}} > 1 \end{cases}$$

Acid base equilibrium conditions

$$ER1 = k_{eq\,w}\left(1 - \frac{S_H S_{OH}}{K_{eq\,w}}\right) \qquad ER4 = k_{eq\,N}\left(S_{NH4} - \frac{S_H S_{NH3}}{K_{eq\,N}}\right) \qquad ER6 = k_{eqS1}(S_{H2S} - \frac{S_H S_{HS}}{K_{eqS1}})$$

$$ER2 = k_{eq\,1}\left(S_{CO2} - \frac{S_H S_{HCO3}}{K_{eq\,1}}\right) \qquad ER5 = k_{eq\,P}\left(S_{H2PO4} - \frac{S_H S_{HPO4}}{K_{eq\,P}}\right) \qquad ER7 = k_{eqS2}(S_{HS} - \frac{S_H S_{S2}}{K_{eqS2}})$$

$$ER3 = k_{eq2}\left(S_{HCO3} - \frac{S_H S_{CO3}}{K_{eq\,2}}\right)$$

Phosphorus binding forms reactions

$$PBR1 = k_{Absorb}\left(Q_{max}\frac{K_{AbsorB2}S_{HPO4}}{(1+K_{AbsorB2}S_{HPO4})} - X_{AbsorbedP}\right) \qquad PBR3 = k_{Fe-P}S_{O2}S_{Fe}$$

$$PBR4 = k_{degFe-P}\frac{K_{O2}^{satur}}{K_{O2}^{satur}+S_{O2}} * X_{Fe-P}$$

$$PBR\ 2 = \frac{S_{Ca}^3 S_{HPO4}^2}{K_{eqApatite} * 10^{-4\,pH}}$$

[1] According to reactions in Table 1-SI.

Table S4. Model parameters and calibration values of the sediment diagenesis model for Lake Simcoe. Table adapted from McCulloch et al. (2013).

Description	Symbol	Value	Units
Proportional Breakdown of Total Sedimentation Flux[#]			
Fraction of OM	α_{Org}	0.42	
Fraction of inorganic matter	α_{Inorg}	1-α_{Org}	
Fraction of inorganic P	α_{Inorg_P}[*]	6.2e-6	
Fraction of redox-sensitive P	$\alpha_{Inorg\_P\_Fe\text{-}P}$[*]	0.33	
Fraction of refractory OM	α_{Org_inert}[*]	0.53	
Fraction of degradable OM	α_{deg}	1- α_{Org_inert}	
Fraction of total settled iron	$\alpha_{Inorg\_Total\ Fe}$	1-(α_{Inorg_Other}+ α_{Inorg_P})	
Fraction of settled FeOOH	$\alpha_{Inorg\_Fe\_FeOOH}$	1-$\alpha_{Inorg\_Fe\_Other}$	
Fraction of settled inorganic Fe, excluding FeOOH	$\alpha_{Inorg\_Fe\_Other}$[*]	0.99	
Fraction of settled apatite P	$\alpha_{Inorg\_P\_ApatiteP}$	1- $\alpha_{Inorg\_P\_Fe\text{-}P}$	
Fraction of inorganic matter without FeOOH and P	α_{Inorg_Other}[*]	0.9999	
Primary redox reactions			
Rate constant of OM degradation with oxygen PR1	k_{O2}[*]	0.024	d^{-1}
Rate constant of OM degradation with nitrate PR2	k_{NO3}[*]	2.09	d^{-1}
Rate constant of OM degradation with manganese oxides PR3	k_{MnO2}[*]	4.33e-6	d^{-1}
Rate constant of OM degradation with iron hydroxides PR4	k_{FeOOH}[*]	3.3e-7	d^{-1}
Rate constant of OM degradation with SO4 PR5	k_{SO4}[1]	1.0e-4	d^{-1}
Half-saturation constant for OM degradation with oxygen	$K_{O_2}^{satur*}$	4.18	mmol/l
Half-saturation constant for OM degradation with nitrate	$K_{NO_3}^{satur*}$	484.7	mmol/l
Half-saturation constant for OM degradation with manganese oxide	$K_{MnO_2}^{satur*}$	0.09	mmol/g
Half-saturation constant for OM degradation with iron hydroxide	K_{FeOOH}^{satur} [*]	0.3	mmol/g
Half-saturation constant for OM degradation with sulfate	$K_{SO_4}^{satur}$ [1]	0.005	mmol/l

Description	Symbol	Value	Units
Secondary redox reactions			
Rate constant for nitrification SR1	k_{nitri} *	0.37	mmol/l/d
Half-saturation constant for nitrification	$K_{nitriNH_4}^{satur}$ *	1.9	mmol/l
Rate of secondary reaction SR2	k_{oxiHS} *	0.001	mmol/l/d
Half-saturation constant for sulfide oxidation	K_{oxiH2S} *	998	mmol/l
Rate of secondary reaction SR3	k_{FeOOHS} [2]	0.1	l/mmol/day
Rate of secondary reaction SR4	k_{FeSO} [2]	55	l/mmol/day
Mineral dissolution and precipitation			
Rate constant for MnCO3 precipitation, MR1	$k_{eqMnCO3prec}$ *	$1.35e^{-5}$	mmol/l/d
Equilibrium constant for MnCO3, MR1	$K_{eqMnCO3}$ [3]	$10^{-10.4}$	$(mmol/l)^2$
Rate constant for MnCO3 dissolution, MR1	$k_{eqMnCO3diss}$ *	0	d^{-1}
Rate constant for CaCO3 precipitation, MR2	$k_{eqCaCO3prec}$ *	0	mmol/l/d
Equilibrium constant for CaCO3, MR2	$K_{eqCaCO3}$ [3]	$10^{(13.87-3059/(273.15+T)-0.04035*(273.15+T))}$	$(mmol/l)^2$
Rate constant for CaCO3 dissolution, MR2	$k_{eqCaCO3diss}$ *	$2.5e^{-7}$	d^{-1}
Rate constant for FeCO3 precipitation, MR3	$k_{eqFeCO3prec}$ *	$1.35e^{-5}$	mol/l/d
Equilibrium constant for FeCO3, MR3	$K_{eqFeCO3}$ [3]	$10^{KeqFeCO3num}$	$(mmol/l)^2$
See above	$K_{eqFeCO3num}$ [3]	-5	
Rate constant for FeCO3 dissolution, MR3	$k_{eqFeCO3diss}$ *	0	d^{-1}
Rate constant for FeS precipitation, MR4	$k_{eqFeSprec}$ [1]	0.002	mmol/l/d
Equilibrium constant for FeS, MR4	K_{eqFeS} [3]	$10^{-12.1}$	$(mmol/l)^2$
Rate constant for FeS dissolution, MR4	$k_{eqFeSdiss}$ [1]	0	d^{-1}
Acid base equilibrium conditions			
Rate constant ER1	k_{eqw} *	1000	d^{-1}
Water dissociation constant	K_{eqw} [3]	$10^{(4470.99/(273.15+T)+12.0875-0.01706*(273.15+T))}$	$(mmol/l)^2$
Rate constant ER2	k_{eq1} *	1000	d^{-1}
Dissociation constant ER2	K_{eq1} [3]	$10^{(14.843-3404.71/(273.15+T)-0.032786*(273.15+T))}$	$(mmol/l)^2$
Rate constant ER3	k_{eq2}	1000	d^{-1}
Dissociation constant ER3	K_{eq2} [3]	$10^{(6.494-2902.39/(273.15+T)-0.02379*(273.15+T))}$	$(mmol/l)^2$
Equilibrium rate constant ER4	k_{eqN} *	1000	d^{-1}
Dissociation constant ER4	K_{eqN} [4]	$10^{(-0.09038-2729/(273.15+T))}$	$(mmol/l)^2$
Equilibrium rate constant ER5	k_{eqP} *	4.72	d^{-1}
Dissociation constant ER5	K_{eqP} [3]	$10^{(-3.46-219.4/(273.15+T))}$	$(mmol/l)^2$
Equilibrium rate constant ER6	k_{eqS1} *	10000	d^{-1}

Description	Symbol	Value	Units
Acid base equilibrium conditions			
Dissociation constant ER6	K_{eqS1}[3]	$10^{(-0.14-1158/(273.15+T))}$	$(mmol/l)^2$
Equilibrium rate constant ER7	k_{eqS2}[*]	10000	d^{-1}
Dissociation constant ER7	K_{eqS2}[3]	$10^{(-2.03-2646/(273.15+T))}$	$(mmol/l)^2$
P Binding Form Reactions			
Adsorption rate, PBR1	k_{Absorb}[*]	0.3	d^{-1}
Adsorption constant, PBR1	K_{Absorb}[5]	118.8	l/mg
Maximal P absorbance sediment capacity, PBR1	Q_{max}[5]	12.7	mg/g
Dissociation constant PBR2	$K_{eqApatite}$[*]	$10^{18.4}$	$(mmol/l)^2$
Rate constant for Fe-P formation, PBR3	$k_{Fe\text{-}P}$[6]	1.5e-4	$mmol^{-1}$ l day^{-1}
Rate constant for Fe-P degradation PBR4	$k_{degFe\text{-}P}$[*]	8.6e-6	d^{-1}
Adsorption rate for Al-P, PBR5	k_{Absorb_Al}[*]	0.3	d^{-1}
Adsorption constant for Al-P, PBR5	K_{Absorb_Al}[5]	1.0	l/mg
Maximal P absorbance sediment capacity for Al-P, PBR5	Q_{max_Al}[7]	0.46	mg/g
Compaction			
Porosity at the SWI	θ_{surf}	0.91	
Porosity at 19.5 cm (core bottom)	θ_{deep}	0.8	
Rate of porosity compaction	k_{θ}[*]	7e-5	d^{-1}
Boundary conditions			
Concentrations at the SWI for dissolved substances			
Oxygen during mixed period	$O_2^{SWI}{}_{high}$	0.30	mmol/l
Oxygen during summer stratified period	$O_2^{SWI}{}_{low}$	0.13	mmol/l
Nitrate, annual average	NO_3^{SWI}	0.022	mmol/l
Ammonium, annual average	$NH_4^{SWI}{}_{mean}$	0.05	mmol/l
Dissolved phosphorus, annual average	$HPO_4^{SWI}{}_{mean}$	7.9e-5	mmol/l
Dissolved manganese	Mn^{SWI}	0.017	mmol/l
Dissolved iron	$\underline{Fe}^{SWI}$	0.008	mmol/l
Sulphate	SO_4^{SWI}	0.03	mmol/l
Dissolved calcium	Ca^{SWI}	1.03	mmol/l
Hydrogen ions	H^{SWI}	6.76e-5	mmol/l
Bicarbonate, HCO_3	HCO_3^{SWI}	3.63	mmol/l
Hydrogen sulphide, HS	HS^{SWI}	0.00	mmol/l
Sulphide S^{2-}	S_2^{SWI}	2.3e-10	mmol/l
Fluxes at the SWI			
Organic matter, annual average	$J_{org,mean}$	0.15	$gDM/m^2/d$
Organic matter, amplitude	$J_{org,amplitude}$	0.04	$gDM/m^2/d$
Manganese oxide, annual average	$J_{MnO2mean}$	1.8e-5	$mol/m^2/d$
Iron hydroxide, annual average	$J_{FeOOHmean}$	4.1e-7	$mol/m^2/d$

Fluxes at the SWI			
Calcium carbonate, annual average	$J_{CaCO3mean}$	2.5e-3	mol/m^2/d
Iron sulfide	J_{FeS}	9.0e-7	mol/m^2/d
Apatite P	$J_{ApatiteP}$	1.8e-6	mol/m^2/d
Iron bound P	$J_{Fe\text{-}P}$	9.0e-7	mol/m^2/d
Aluminium bound P	$J_{Al\text{-}P}$	9.0e-7	mol/m^2/d
Molecular diffusion coefficients			
Dynamic viscosity	mu	0.01*(1.791-0.06144*T +0.001451*T^2 -1.6826*10^{-5}*T^3 -0.0001529*p+8.3885*10^{-8}*p^2 +0.0024727*S+T*(6.0574*10^{-6}*p -2.676*10^{-9}*p^2)+S*(4.48429*10^{-5}*T -4.7172*10^{-6}*T^2+7.5986*10^{-8}*T^3))	poise
Temperature	T		^{o}C
Water pressure	P	1.01325+0.0980665*Depth	bar
Salinity	S	0.15	g/kg
Molecular diffusion coefficients for Ca^{2+}	$D_{S\ Ca}$	(3.6+0.179*T)*10-6*8.64	m^2/d
Molecular diffusion coefficients for CO_2	$D_{S\ CO2}$	4.72*10-9*(273.15+T)/ /(mu*37.3$^{0.6}$)*8.64	m^2/d
Molecular diffusion coefficients for Fe^{2+}	$D_{S\ Fe}$	(3.31+0.15*T)*10-6*8.64	m^2/d
Molecular diffusion coefficients for HPO_4^-	$D_{S\ HPO4}$	(3.26+0.177*T)*10-6*8.64	m^2/d
Molecular diffusion coefficients for NH_4^+	$D_{S\ NH4}$	(9.5+0.413*T)*10-6*8.64	m^2/d
Molecular diffusion coefficients for O_2	$D_{S\ O2}$	4.72*10-9*(273.15+T)/ /(mu*27.9$^{0.6}$)*8.64	m^2/d
Molecular diffusion coefficients for Mn^{2+}	$D_{S\ Mn}$	(3.18+0.155*T)*10-6*8.64	m^2/d
Molecular diffusion coefficients for SO_4^{2-}	$D_{S\ SO4}$	(4.88+0.232*T)*10-6*8.64	m^2/d
Bioturbation coefficient	D_b	30	cm^2/year
Bioirrigation coefficient	$\alpha_{bioirrig}$	1.0e-7	s^{-1}

[#] According to Fig. 3 in McCulloch et al. (2013);

* Denotes fitted parameter. DM indicates dry matter and OM indicates organic matter.

[1] Dittrich et al. (2009), [2] Katsev et al. (2006), [3] Stumm and Morgan (1996), [4] Clegg and Whitfield (1995), [5] Dong et al. (2011), [6] Reed et al. (2011), [7] Kopáček et al. (2005).

Table S5. Correlation matrix of the model parameters*. Correlation coefficients with absolute value higher than 0.50 are reported in bold font.

	O_2^{SWI}	α_{Org_inert}	α_{Org}	k_{O2}	$K^{satur}{}_{O2}$	J_{CaCO3}	k_θ	NO_3^{SWI}	D_B	k_{NO3}	$K^{satur}{}_{NO3}$	$\alpha_{bioirrig}$	HCO_3^{SWI}	Ca^{SWI}	H^{SWI}	$k_{oxi\ HS}$	HS^{SWI}	Fe^{SWI}	Mn^{SWI}	k_{FeOOH}	K_{FeOOH}	$k_{degFe-P}$	k_{Fe-P}	k_{nitri}
O_2^{SWI}	**1.00**	-0.20	0.14	0.00	-0.02	-0.01	0.03	**-0.76**	-0.12	0.13	0.18	**-0.61**	**0.97**	-0.08	-0.04	0.07	-0.02	-0.24	-0.11	0.40	-0.10	0.17	0.06	-0.34
α_{Org_inert}	-0.20	**1.00**	0.02	-0.06	-0.23	0.15	-0.24	-0.08	-0.18	-0.04	-0.13	0.27	-0.11	0.04	0.03	-0.10	0.02	0.05	0.08	-0.06	0.02	-0.01	0.00	0.28
α_{Org}	0.14	0.02	**1.00**	0.00	0.11	0.13	0.18	0.05	0.14	-0.05	0.01	-0.18	0.08	-0.03	-0.02	0.06	-0.01	-0.05	-0.06	-0.04	0.02	0.05	0.05	-0.19
k_{O2}	0.00	-0.06	0.00	**1.00**	**0.97**	0.03	0.10	0.19	**0.61**	-0.14	-0.17	0.27	-0.05	-0.05	-0.03	**0.83**	0.02	-0.18	-0.15	0.16	**0.60**	-0.25	**-0.74**	-0.25
$K^{satur}{}_{O2}$	-0.02	-0.23	0.11	**0.97**	**1.00**	-0.01	0.18	0.20	**0.61**	-0.18	-0.18	0.27	-0.06	-0.04	-0.02	**0.83**	0.02	-0.17	-0.15	0.16	**0.58**	-0.29	**-0.72**	-0.24
J_{CaCO3}	-0.01	0.15	0.13	0.03	-0.01	**1.00**	0.13	-0.01	0.00	-0.05	-0.07	0.03	-0.01	0.01	0.00	0.02	0.00	0.00	0.04	-0.01	-0.02	0.00	0.03	0.02
k_θ	0.03	-0.24	0.18	0.10	0.18	0.13	**1.00**	0.16	0.03	-0.01	0.02	-0.24	-0.04	-0.02	0.03	0.05	-0.02	0.00	-0.01	-0.05	-0.19	-0.43	0.11	-0.10
NO_3^{SWI}	**-0.76**	-0.08	0.05	0.19	0.20	-0.01	0.16	**1.00**	0.47	0.05	-0.02	0.21	**-0.89**	0.01	0.00	0.03	-0.01	0.14	0.02	-0.43	0.15	-0.08	-0.06	-0.11
D_B	-0.12	-0.18	0.14	**0.61**	**0.61**	0.00	0.03	0.47	**1.00**	-0.22	-0.19	0.39	-0.20	-0.06	0.15	0.45	0.00	-0.10	-0.03	-0.04	0.35	-0.30	-0.24	-0.35
k_{NO3}	0.13	-0.04	-0.05	-0.14	-0.18	-0.05	-0.01	0.05	-0.22	**1.00**	**0.98**	-0.45	0.03	-0.15	-0.11	**-0.51**	-0.04	-0.01	0.10	0.20	0.04	**0.58**	0.19	-0.17
$K^{satur}{}_{NO3}$	0.18	-0.13	0.01	-0.17	-0.18	-0.07	0.02	-0.02	-0.19	**0.98**	**1.00**	-0.42	0.11	-0.16	-0.10	**-0.53**	-0.04	-0.02	0.12	0.26	0.00	**0.52**	0.24	-0.16
$\alpha_{bioirrig}$	**-0.61**	0.27	-0.18	0.27	0.27	0.03	-0.24	0.21	0.39	-0.45	-0.42	**1.00**	-0.45	0.07	0.19	0.23	0.04	0.09	0.13	-0.04	0.25	-0.43	-0.22	0.40
HCO_3^{SWI}	**0.97**	-0.11	0.08	-0.05	-0.06	-0.01	-0.04	**-0.89**	-0.20	0.03	0.11	-0.45	**1.00**	-0.06	0.02	0.06	-0.02	-0.22	-0.08	0.44	-0.12	0.11	0.07	-0.20
Ca^{SWI}	-0.08	0.04	-0.03	-0.05	-0.04	0.01	-0.02	0.01	-0.06	-0.15	-0.16	0.07	-0.06	**1.00**	0.00	-0.05	0.00	-0.01	0.00	-0.42	0.00	-0.07	0.10	-0.09
H^{SWI}	-0.04	0.03	-0.02	-0.03	-0.02	0.00	0.03	0.00	0.15	-0.11	-0.10	0.19	0.02	0.00	**1.00**	-0.02	0.00	-0.01	0.04	-0.02	0.02	-0.08	0.06	0.04
$k_{oxi\ HS}$	0.07	-0.10	0.06	**0.83**	**0.83**	0.02	0.05	0.03	0.45	**-0.51**	**-0.53**	0.23	0.06	-0.05	-0.02	**1.00**	0.04	-0.14	-0.33	0.09	**0.56**	-0.25	**-0.86**	-0.02
HS^{SWI}	-0.02	0.02	-0.01	0.02	0.02	0.00	-0.02	-0.01	0.00	-0.04	-0.04	0.04	-0.02	0.00	0.00	0.04	**1.00**	0.01	0.00	-0.11	-0.04	0.00	-0.02	0.06
Fe^{SWI}	-0.24	0.05	-0.05	-0.18	-0.17	0.00	0.00	0.14	-0.10	-0.01	-0.02	0.09	-0.22	-0.01	-0.01	-0.14	0.01	**1.00**	0.03	-0.17	-0.11	-0.03	0.11	0.16
Mn^{SWI}	-0.11	0.08	-0.06	-0.15	-0.15	0.04	-0.01	0.02	-0.03	0.10	0.12	0.13	-0.08	0.00	0.04	-0.33	0.00	0.03	**1.00**	-0.05	-0.15	-0.10	0.26	0.10
k_{FeOOH}	0.40	-0.06	-0.04	0.16	0.16	-0.01	-0.05	-0.43	-0.04	0.20	0.26	-0.04	0.44	-0.42	-0.02	0.09	-0.11	-0.17	-0.05	**1.00**	0.06	0.01	-0.09	-0.02
K_{FeOOH}	-0.10	0.02	0.02	**0.60**	**0.58**	-0.02	-0.19	0.15	0.35	0.04	0.00	0.25	-0.12	0.00	0.02	**0.56**	-0.04	-0.11	-0.15	0.06	**1.00**	0.29	**-0.74**	-0.19
$k_{degFe-P}$	0.17	-0.01	0.05	-0.25	-0.29	0.00	-0.43	-0.08	-0.30	**0.58**	**0.52**	-0.43	0.11	-0.07	-0.08	-0.25	0.00	-0.03	-0.10	0.01	0.29	**1.00**	-0.10	-0.06
k_{Fe-P}	0.06	0.00	0.05	**-0.74**	**-0.72**	0.03	0.11	-0.06	-0.24	0.19	0.24	-0.22	0.07	0.10	0.06	**-0.86**	-0.02	0.11	0.26	-0.09	**-0.74**	-0.10	**1.00**	-0.21
k_{nitri}	-0.34	0.28	-0.19	-0.25	-0.24	0.02	-0.10	-0.11	-0.35	-0.17	-0.16	0.40	-0.20	-0.09	0.04	-0.02	0.06	0.16	0.10	-0.02	-0.19	-0.06	-0.21	**1.00**

* Based on the IDENT procedure from UNCSIM software package (Reichert, 2005). The matrix is part of the identifiability analysis presented in detail by McCulloch et al. (2013). Each parameter is varied within 10% of its standard deviation under the assumption of a normal distribution. The standard deviations of S_i concentrations are proportional to values of scaling parameters to make concentrations of different species comparable (McCulloch et al., 2013). For more details, the reader is referred to the links http://www.uncsim.eawag.ch/ and http://www.eawag.ch/forschung/siam/software/ident/index

References

Clegg, S.L., and Whitfield, M., 1995. A chemical model of seawater including dissolved ammonia and the stoichiometric dissociation constant of ammonia in estuarine water and seawater from− 2 to 40° C. Geochim Cosmochim Ac. 59, 2403-2421.

Dittrich, M., Wehrli, B., and Reichert, P., 2009. Lake sediments during the transient eutrophication period: Reactive-transport model and identifiability study. Ecol. Model. 220, 2751-2769.

Dong, L., Yang, Z., and Liu, X., 2011. Phosphorus fractions, sorption characteristics, and its release in the sediments of Baiyangdian Lake, China. Environ Monit Assess. 179, 335-345.

Katsev, S., Tsandev, I., L'Heureux, I., and Rancourt, D.G., 2006. Factors controlling long-term phosphorus efflux from lake sediments: Exploratory reactive-transport modeling. Chem. Geol. 234, 127-147.

Kopáček, J., Borovec, J., Hejzlar, J., Ulrich, K.-U., Norton, S.A., and Amirbahman, A., 2005. Aluminum control of phosphorus sorption by lake sediments. Environ Sci Technol. 39, 8784-8789.

McCulloch, J., Gudimov, A., Arhonditsis, G., Chesnyuk, A., and Dittrich, M., 2013. Dynamics of P-binding forms in sediments of a mesotrophic hard-water lake: Insights from non-steady state reactive-transport modelling, sensitivity and identifiability analysis. Chem Geol. 354, 216-232.

Reed, D.C., Slomp, C.P., and Gustafsson, B.G., 2011. Sedimentary phosphorus dynamics and the evolution of bottom-water hypoxia: A coupled benthic-pelagic model of a coastal system: Limnol and Oceanogr. 56, 1075-1092.

Reichert, P., 2005, UNCSIM a computer programme for statistical inference and sensitivity, identifiability, and uncertainty analysis. In: Teixeira, J.M.F., Carvalho-Brito, A.E. (Eds.), Proceedings of the 2005 European Simulation and Modelling Conference (ESM 2005), October 24–26, Porto, Portugal, EUROSIS-ETI. pp. 51–55.

Stumm, W., and Morgan, J., 1996. Aquatic chemistry, chemical equilibria and rates in natural waters. 3rd ed. John Wiley & Sons, Inc., New York (1022p).